International Journal of Microwave and Wireless Technologies

cambridge.org/mrf

Research Paper

Cite this article: Nayak VSP, Manjunathachari K (2025) Design and analysis of the triple band circular quarter mode substrate integrated waveguide (QMSIW) 1 × 2 MIMO antenna. International Journal of Microwave and Wireless Technologies, 1–20. https://doi.org/10.1017/S1759078725102286

Received: 2 February 2025 Revised: 22 August 2025 Accepted: 4 September 2025

Keywords:

Circular Quarter Mode Substrate Integrated waveguide (CQMSIW); Multi Input Multi Output (MIMO); sub-6 GHz 5 G Applications

Corresponding author:

V. Shiva Prasad Nayak; Email: svadthya@gitam.edu

© The Author(s), 2025. Published by Cambridge University Press in association with The European Microwave Association. This is an Open Access article, distributed under the terms of the Creative Commons Attribution licence (http://creativecommons.org/licenses/by/4.0), which permits unrestricted re-use, distribution and reproduction, provided the original article is properly cited.



Design and analysis of the triple band circular quarter mode substrate integrated waveguide (QMSIW) 1 × 2 MIMO antenna

V. Shiva Prasad Nayak (b) and K. Manjunathachari

Department of EECE, GITAM (Deemed to be) University, Hyderabad, India

Abstract

This paper presents the design and analysis of the Triple band Circular Quarter Mode Substrate Integrated Waveguide (QMSIW) 1 × 2 MIMO antenna for sub-6 GHz 5 G wireless applications. The antenna operates at three distinct frequencies those are 3.57GHz, 4.41GHz and 5.43 GHz respectively. The 3.57 GHz used to operate for WiMAX, 5 G, and Fixed Wireless Access, the 4.41 GHz, is often used for specific satellite uplink/downlink operations, Radar Systems and the third one 5.43 GHz is used for Wi-Fi, DSRC, and WLAN systems. The proposed architectural design underwent simulation utilizing electromagnetic (EM) tools to the extract results, followed by antenna fabrication and measured results, it was observed that there is a close match between the simulation, measured results and validated results. The measured, simulation gain values are 5.092dBi,4.98dBi at 3.57 GHz, 4.51dBi,4.6dBi at 4.41 GHz and 3.075dBi,3.06dBi at 5.43 GHz frequency, while also demonstrating satisfactory isolation between the ports, quantified as being less than -15 dB. The characteristic parameters of the MIMO antenna, including a diversity-gain (DG) surpassing 9.95 dB (>9.95 dB), alongside an envelope-correlation-coefficient (ECC) of less than 0.0001, Mean effective gain (MEG) lies between - 3 dB to - 4 dB, among any two radiating elements at every operational frequency, indicate that the antenna has been meticulously designed.

Introduction

As a backbone to modern wireless communication, antennas are widely used for signal transmission and reception. In Recent days, antennas are designed for Sub-6 GHz applications to play an important role in high-speed connectivity and enabling reliable. The sub-6 GHz frequencies have a variety of applications like WiMAX applications, 5G, and Fixed Wireless Access, satellite uplink/downlink operations, Radar Systems, and WLAN systems, etc. and also enabling advanced applications like driverless vehicles, virtual reality and smart cities. These bands offer a balance between data rate and coverage, making them essential for indoor and wide-area communication systems [1, 2].

The operational frequency bands encompass 3.3 to 3.6 in China and India, 3.4 to 3.8 GHz in the UK, 3.45 to 3.7 GHz in the United States, 4.4 to 4.9 GHz in Japan, and 4.8 to 5 GHz in China, all of which fall under the sub-6 GHz category; moreover, the Federal Communications Commission (FCC) has allocated several additional bands, including 24 GHz, 28 GHz, 37 GHz, 39 GHz, 47 GHz, 60 GHz, and 79 GHz [3–5], all of which are designated as unlicensed bands available for public access. The increasing prominence of these frequency bands can be attributed to advancements in high throughput, minimal latency, reduced power consumption, cost-effectiveness, and shorter operational ranges.

Antennas operating at distinct frequencies are used for distinct applications, to improve technological advancement. As a part of wireless communication technology, the use of a single antenna for multiple purposes has become the most popular in today's world. Since antennas are important to modern day communication gadgets, A number of multi-band antenna systems have been designed and developed to accommodate specific applications in a single device. But multi-purpose antennas undergo coupling issues which affect antenna performance. In order to overcome this problem, research on dual and triple-band antennas has boomed in recent times. Moreover, integrating slots on patch for dual band and triple band frequencies enables multipurpose applications but is always challenging due to fixed frequency requirements, where antenna dimensional adjustments impact overall antenna performance, especially in case of triple-band scenarios [6].

Due to smaller wavelengths at high frequencies and tight tolerances in high frequency antenna applications the use of microstrip antenna devices is not efficient. Hence waveguide devices are chosen at higher frequencies. But the manufacturing process of waveguide devices

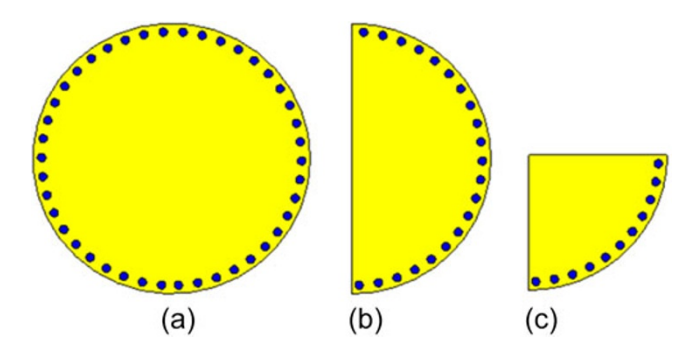


Figure 1. Design evaluation of circular QM-SIW.

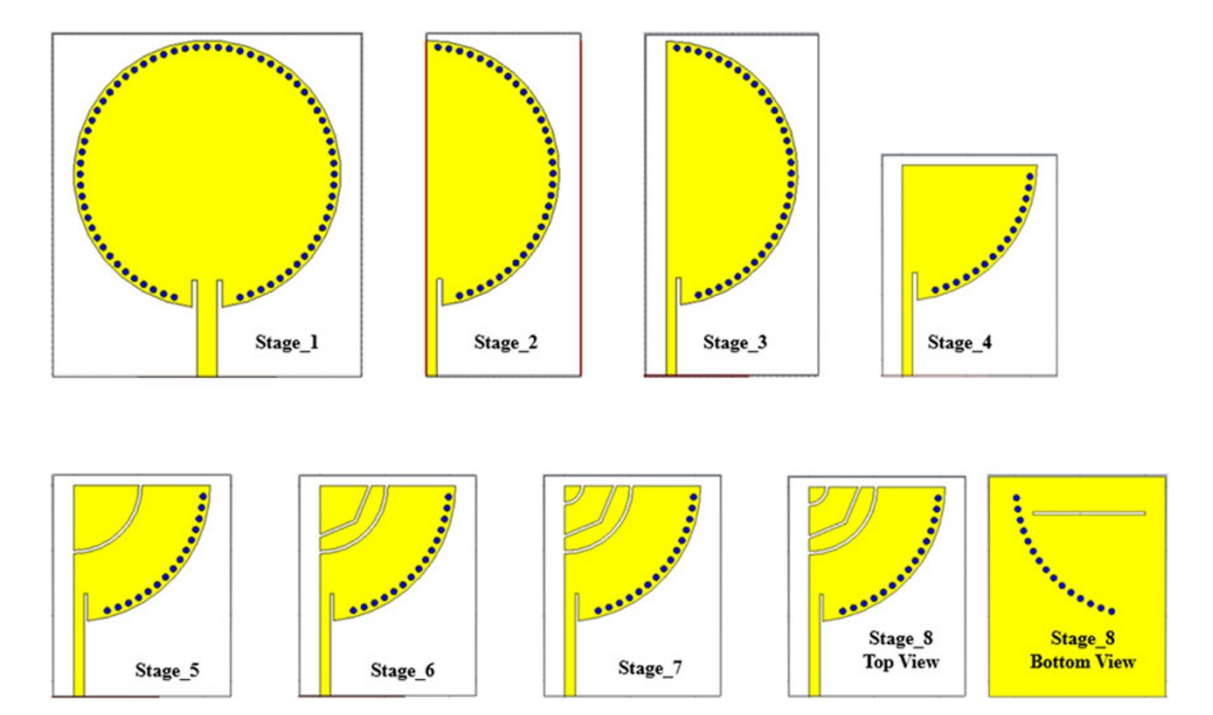


Figure 2. Design evaluation of the proposed design.

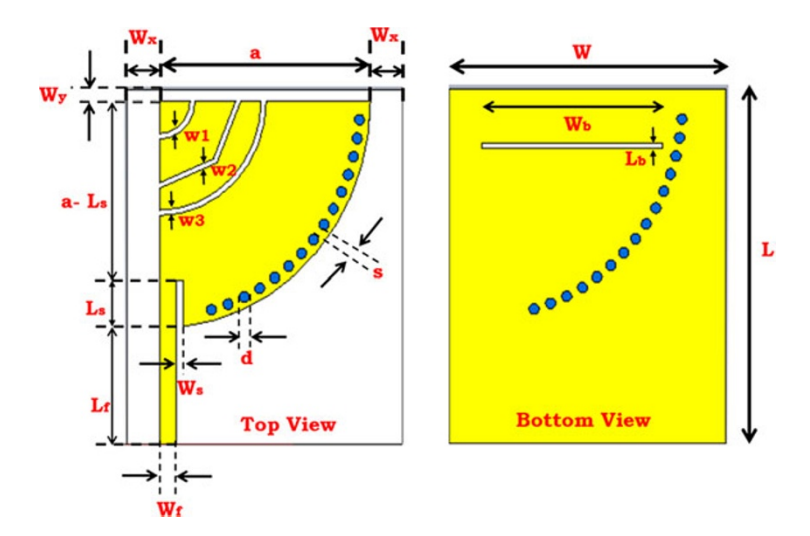


Figure 3. Parameter representation Circular QM-SIW.

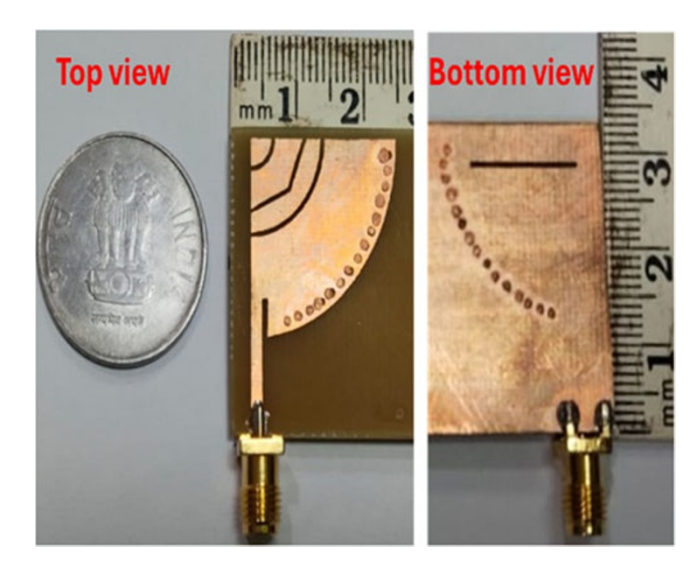


Figure 4. Fabricated prototype.

Table 1. Parameters used in this antenna

Parameter	Value (mm)	Parameter	Value (mm)	
W	27	W_f	1.6	
L	33.5	L _f	11.5	
W _m	54	W_s	0.75	
L _m	33.5	$w1=w2=w3=L_b$	0.5	
W _b	17.5	L _s	4.3	
a	21	W _x	3	
d/s	1/1.6	W _y	1	

is very difficult. Hence a new concept called substrate integrated waveguide (SIW) was introduced. SIW is a transformation between microstrip, and dielectric filled waveguide (DFW) and is transformed to SIW by interconnecting the patch and lower metallic

ground planes with periodic arrays of metallic vias through the dielectric substrate [7, 8].

The slot antenna is perfect for wireless usage since it is lighter, smaller, and simpler to fabricate than the other types of antennas, such as the array and horn antennas. SIW technology has enabled the implementation of SIW slot antennas [9]. The design features are further improved by moving to cavity-backed antennas, which have smaller size, better bandwidth, and moderate gain.

A new concept, QMSIW has been proposed, with a view for attaining size minimisation. The SIW can be divided into two halves, by including a symmetric magnetic wall to intersect the SIW structure transversely. Each half forms an Half-Mode Substrate Integrated Waveguide (HMSIW) structure [2], then HMSIW can be divided into two halves, by including a symmetric magnetic wall to intersect the SIW structure transversely. Each half forms an QMSIW structure, which is in principle able to support quarter-guided wave modes coils. Each quarter forms an QMSIW structure, which is in principle able to support quarter-guided wave modes coils. As a result, one-quarter of the original structure is maintained, which leads to a size reduction of 75% in comparison to the traditional SIW cavity which is shown in Fig. 1.

Multiple Input Multiple Output (MIMO) technology has completely changed the face of wireless communication systems. It forms the core of recent and future higher generations of wireless communication systems, namely 3G, 4G, 5G, and 6G [10-12] Now, 5G has been launched worldwide with a promise to provide higher data rates, lower latency with huge capacity, favouring the exchange of information in real time. Therefore, MIMO antennas with diverse capabilities are in demand and have been utilized by several researchers [13-17]. Basically, the MIMO antenna should be capable enough to serve several simultaneous applications to maintain compact size of the system. Therefore, the integration of MIMO technology with multiband capability gives a striking solution to this limitation of MIMO antennas. Apart from MIMO capability, microstrip technology can also provide multiband performance. The use of this technology also provides ease of integrating antennas with a communication system.

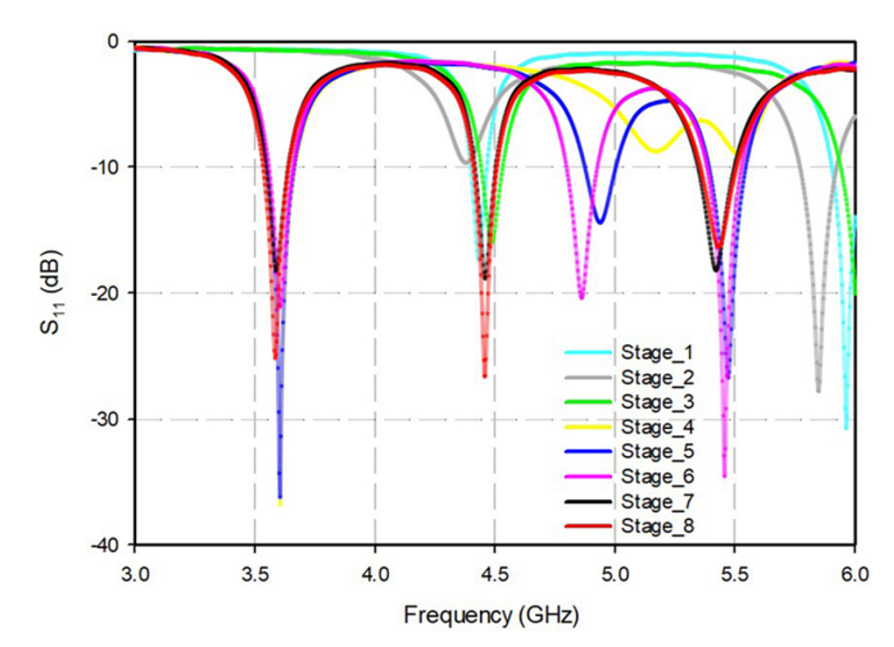


Figure 5. S_{11} results for different stages of the proposed design.

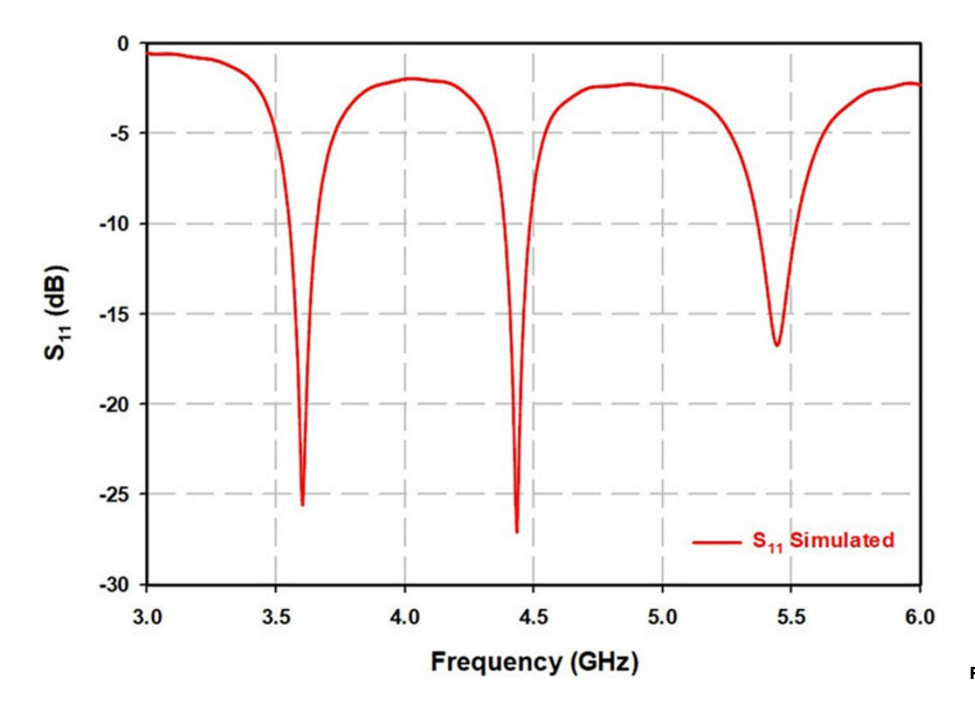


Figure 6. Reflection Coefficient.

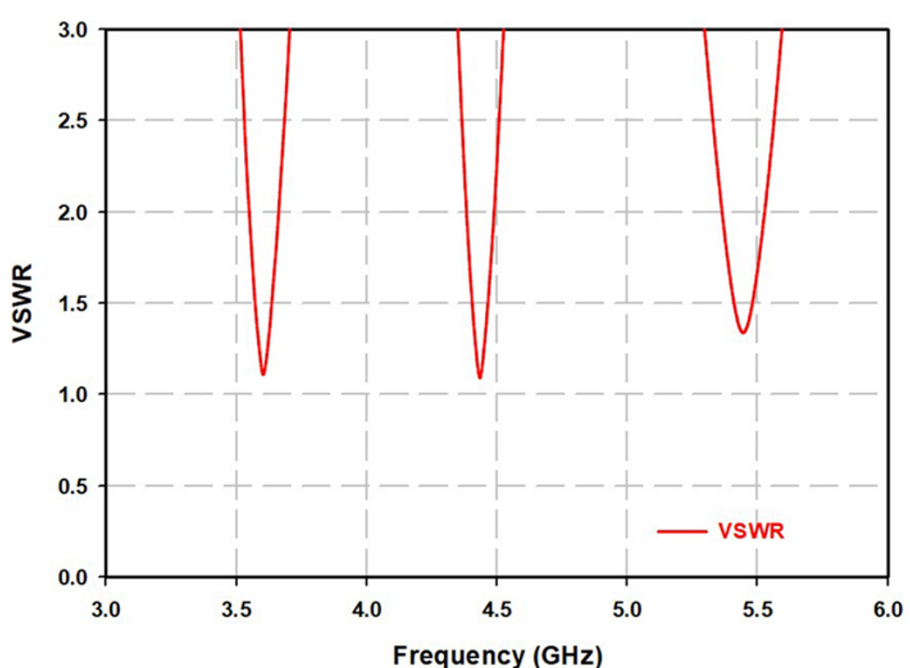


Figure 7. VSWR.

The suggested method discusses the circular QMSIW 1×2 MIMO antenna to function under sub 6 GHz 5G applications. The section 2 discusses the conversion processes of QMSIW and their simulation results and validation results and also emphasis the discussion of the results of 1×2 MIMO-based antenna and parameters like DG and ECC are reported in section 3, and the analysis, conclusions, and future scope of this work are described in further sections.

The proposed 1×2 MIMO antenna has been designed and optimized to appeal as follows.

1. For sub-6 GHz 5G Applications, the proposed Circular Quarter Mode Substrate Integrated Waveguide (QMSIW) 1×2 MIMO

antenna has been developed utilizing a substrate loaded with one octagonal and two circular slots loaded on the patch and one rectangular slot is loaded on the ground plane.

- 2. The designed antenna is portable in size, easier to build, comparatively weightless and budget friendly.
- 3. Operating at three different frequencies 3.57 GHz, 4.41 GHz and 5.43 GHz with improved return loss.
- 4. Attained gain 4.98dBi at 3.57 GHz, 4.6dBi at 4.41 GHz, 3.06dBi at 5.43 GHz and stable radiation patterns.
- 5. Attained ECC is below 0.0001 (ECC < 0.0001), DG is more than 9.995 dB (DG > 9.95 dB) and MEG lies between 3 dB to 4 dB for all operating frequency bands.

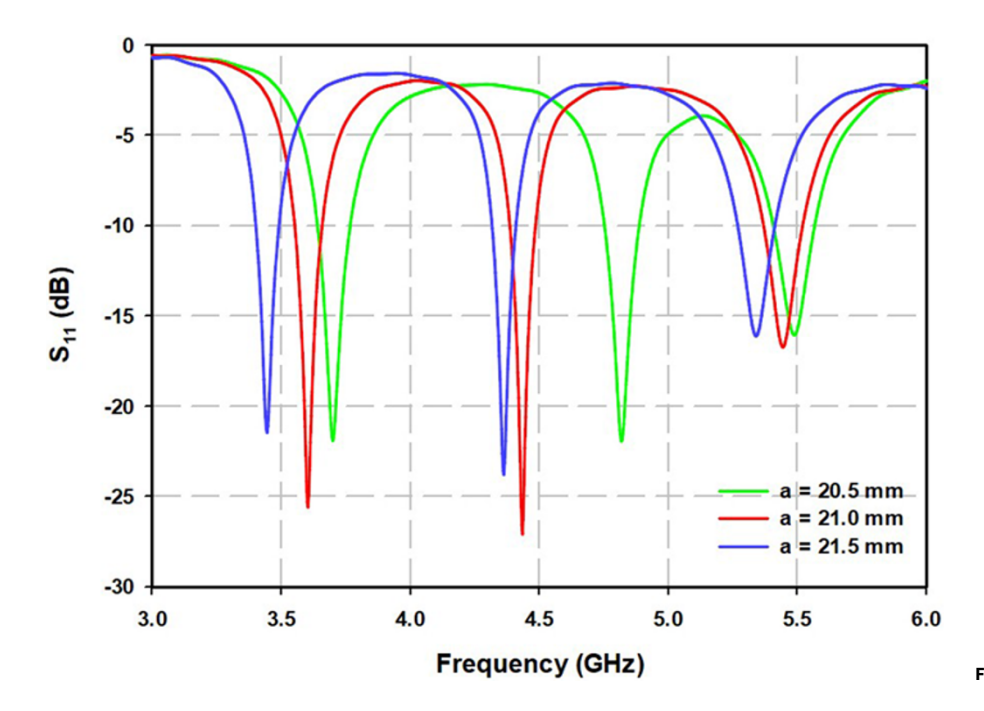


Figure 8. S_{11} for different values of SIW width (a).

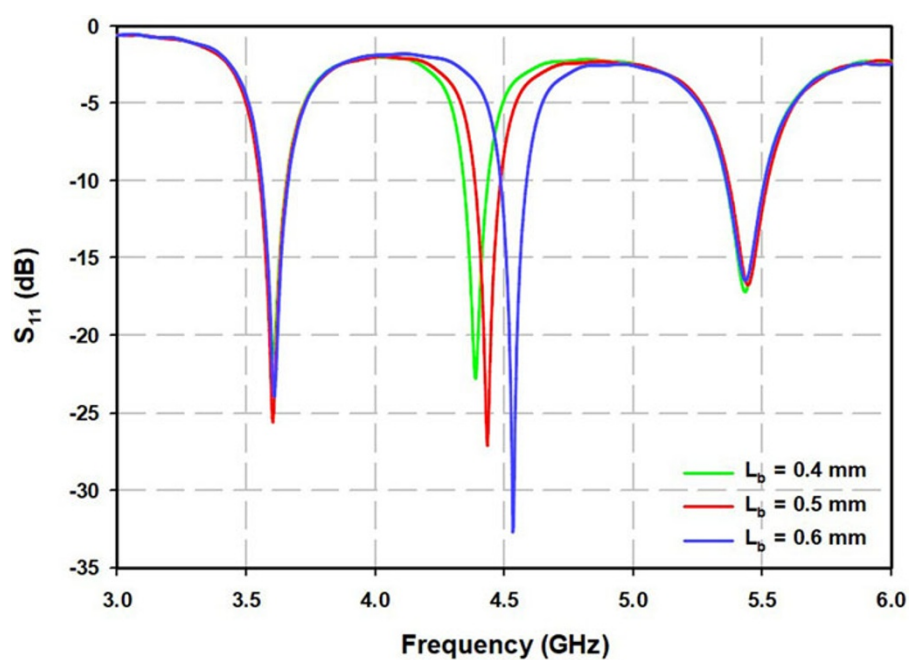


Figure 9. S_{11} for different values of bottom side rectangular slot width (L_b) .

Quarter mode substrate integrated waveguide (QMSIW)

Figure 1 illustrates the design evaluation of the proposed design to achieve the size reduction and Fig. 1a shows the circular-shaped SIW cavity-backed antenna. It can be split into two parts either horizontally or vertically for size reduction as named as circular half-mode SIW (CHMSIW) represented in Fig. 1b and further split into two parts named as circular Quarter Mode SIW (CQMSIW) antenna represented in Fig. 1c. The material used for developing proposed design is FR-4 with a dielectric constant of 4.4 with a thickness of 1.6 mm. The electromagnetic tool is used employed to assess the antenna performance in terms of S_{11} , gain, surface current, voltage standing wave ratio (VSWR), and far-field radiation pattern

The Fig. 2 represents the design evaluation of the proposed antenna and their design steps are as follows

Stage 1: Design a circular shaped SIW fed by microstrip

Stage 2: Convert SIW to HMSIW by cutting horizontally by two parts

Stage 3: Extend the substrate of HMSIW.

Stage 4: Convert HMSIW to QMSIW by cutting vertically two parts

Stage 5: Insert Quarter shape of circle in QMSIW

Stage 6: Load Quarter shape octagonal loaded in top of the substrate and before to circle slot

Stage 7: Load Quarter shape circle slot loaded in top of the substrate and before to octagonal slot

Stage 8: Finally, introducing rectangular slot in bottom of the substrate for accuracy improvement

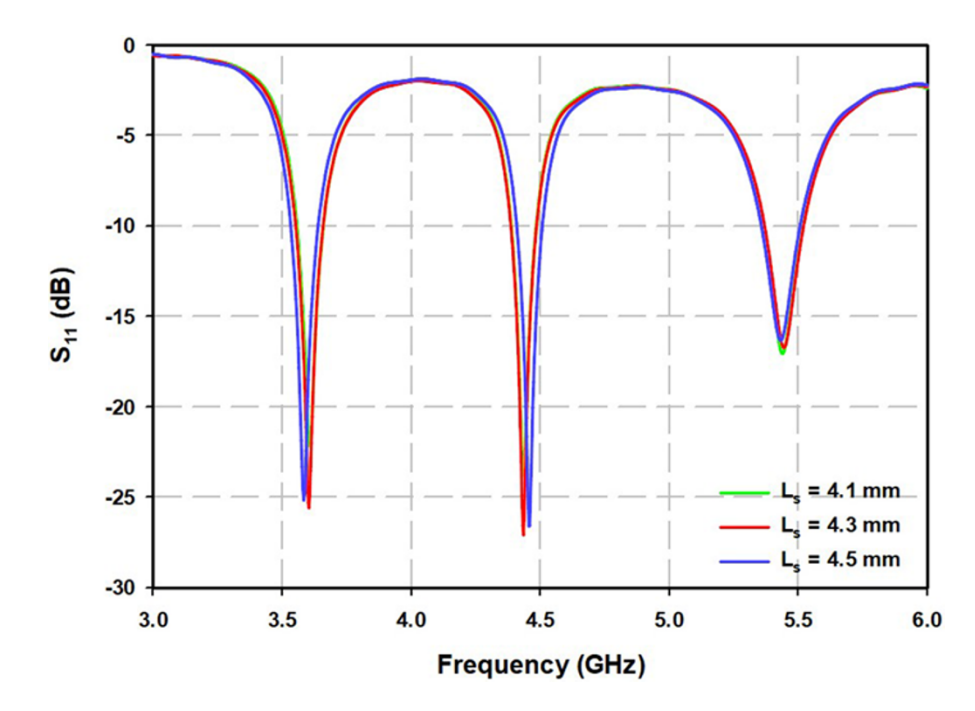


Figure 10. S_{11} for different values of strip substrate length (L_c).

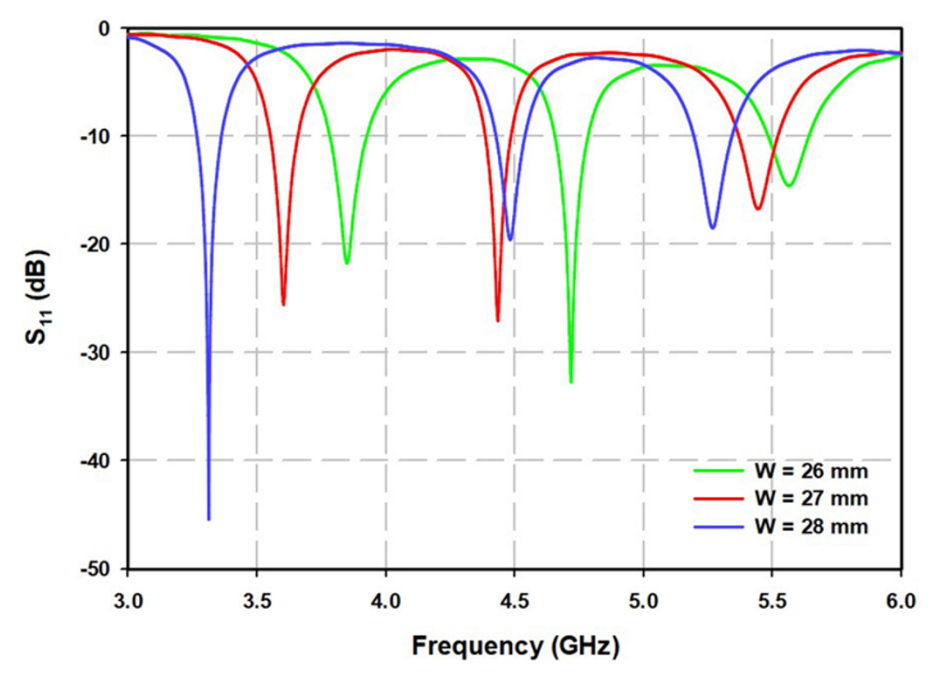


Figure 11. S_{11} for different values of width (W).

The Fig. 3 shows a parametric representation of the proposed design where the left side indicates the top view and the right side indicates the bottom view. The microstrip feed line used in this design and has 50ohms characteristics impedance. In the top view, two circle slots are loaded in the middle of the substrate and an octagonal slot is loaded in between two circular slot and rectangular slots are loaded in the back side of the proposed antenna and their dimension is $27 \times 33.5 \times 1.6$ mm³. The Fig. 4 represents the printed prototype in which the right side belongs to the bottom view and the left side belongs to the top view. Table 1 intensifies the parameters used in this design.

The SIW cavity is cylindrical in nature, so the design frequency and working principle can be calculated from the solution of the wave equation in a cylindrical cavity with few modifications due to the discontinuous sidewall. If we neglect the leakage of the sidewall, the resonant frequency of the ${\rm TM}_{\rm npq}$ mode of a cylindrical cavity, having radius (a) and height (d), is represented in eq. 1 [18].

$$f_r = \frac{C}{2\Pi\sqrt{\mu_r\varepsilon_r}}\sqrt{\left(\frac{X_{np}}{a}\right)^2 + \left(\frac{q_\Pi}{d}\right)^2} \tag{1}$$

where X_{np} tells the P_{th} zero of the n_{th} order Bessel function of the first kind. For the fundamental TM_{010} mode, in the context of a circular SIW cavity, the resonant frequency can be articulated as

$$f_{010} = \frac{2.405C}{2\Pi a \sqrt{\mu_r \varepsilon_r}} \tag{2}$$

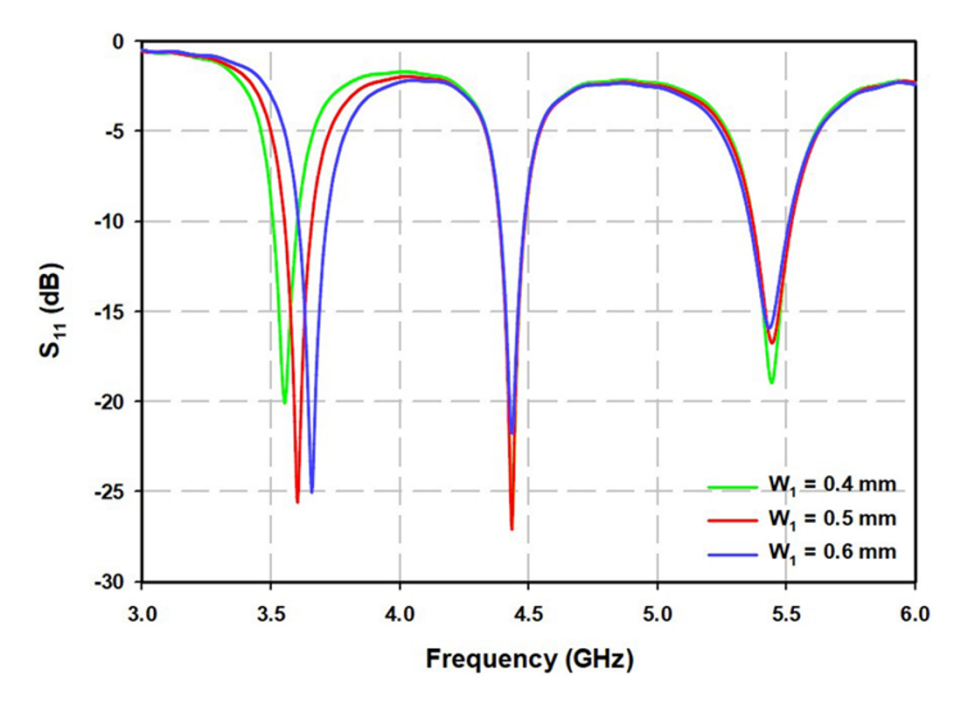


Figure 12. S_{11} for different values of first circle width (W_1) .

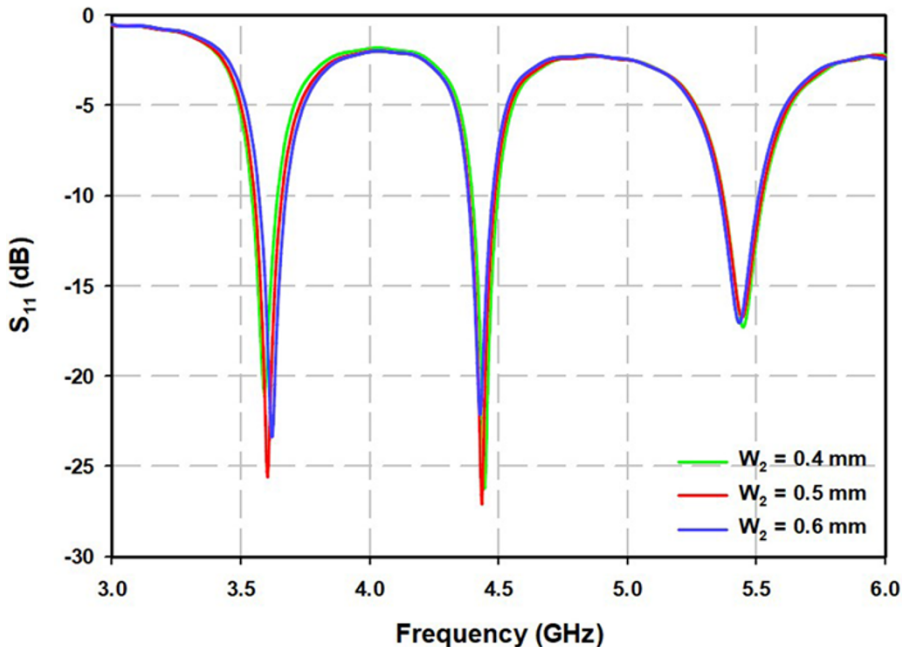


Figure 13. S_{11} for different values of octagonal slot width (W_2) .

The frequency of resonance achieved is calculated to be $3.2\,\mathrm{GHz}$ when the parameter a (representing the radius of the cavity) is assigned a value of $18.15\,\mathrm{mm}$. The diameter (d) and spacing (s) between the adjacent metallic via are two key parameters of the SIW of the metallic via is represented in eq. $3\,[2,8]$.

$$d \leqslant \frac{\lambda_g}{5} \text{ and } s \leqslant 2d$$
 (3)

The reflection coefficient of the proposed design for different stages is represented in Fig. 5 over the frequency range 3 to 6 GHz. Final proposed antenna as good accuracy comparing with all the stages and resonates at 3.57 GHz, 4.41 GHz and 5.43 GHz respectively. The S₁₁ of the proposed antenna is shown in Fig. 6 over

the frequency range 3 to 6 GHz and it is operated in three frequencies i.e. 3.57 GHz, 4.41 GHz, 5.43 GHz and their $\rm S_{11}$ values are -23.66 dB -25.44 dB, -16.10 dB. The operating bandwidth of the proposed design is 110 MHz at 3.57 GHz resonant frequency (3.52 GHz to 3.63 GHz), 100 MHz at 4.41 GHz resonant frequency (4.36 GHz to 4.46 GHz), 150 MHz at 5.43 GHz resonant frequency (5.35 to 5.50 GHz) concerning - 10 dB baseline and well suited to operate in WLAN, Wi-MAX, Wi-Fi, radar systems and sub-GHz 5 G Applications.

The Fig. 7 represents the VSWR of the proposed design and produces three resonant frequencies 3.57 GHz, 4.41 GHz and 5.43 GHz respectively, has VSWR of 1.141, 1.118 and 1.367. The VSWR results (2:1 ratio) matched with S_{11} result. The parametric variation of SIW Width S_{11} result is revealed in Fig. 8 over

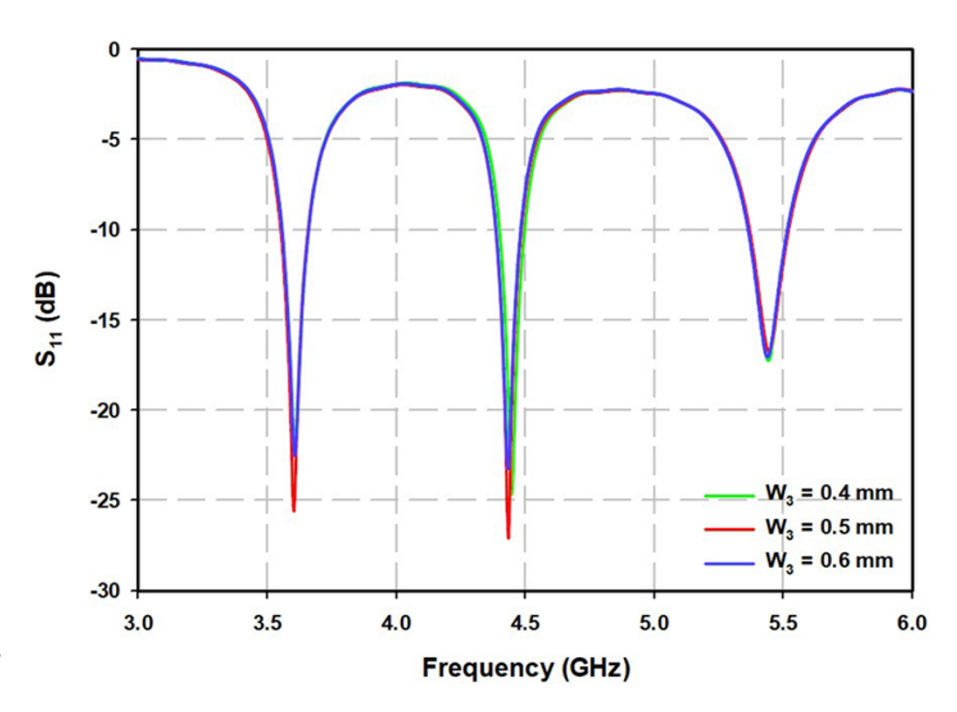


Figure 14. S_{11} for different values of second side circle slot width (W_3) .

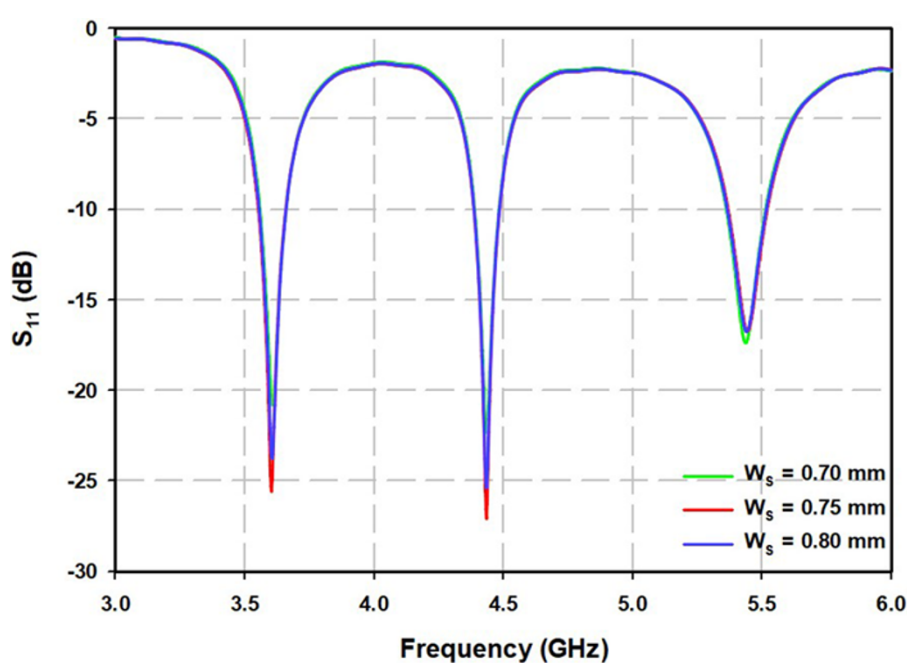


Figure 15. S_{11} for different values of bottom rectangular slot width (W_s).

the range of frequencies 3 to 6 GHz. The three values are taken for analysing the performance of the S_{11} and those are 20.5 mm, 21 mm, 21.5 mm, represented by green, red and blue colours. The change in SIW width will affect the accuracy and resonant frequency. The best value chosen is 21 mm and has better accuracy and operated in three frequencies 3.57 GHz, 4.41 GHz and 5.43 GHz.

The parametric variation of bottom side rectangular slot width S_{11} result is revealed in Fig. 9 over the range of frequencies 3 to 6 GHz. The three values are taken for analysing the performance of the S_{11} and those are 0.4 mm, 0.5 mm, 0.6 mm, represented by green, red and blue colours. The change in bottom side rectangular slot width will affect the change in second resonant frequency. The best value chosen is 0.5 mm.

The parametric variation of strip length (L_s) S_{11} result is revealed in Fig. 10 over the range of frequencies 3 to 6 GHz. The three values are taken for analysing the performance of the S_{11} and those are 4.1 mm, 4.3 mm, 4.5 mm, represented by green, red and blue colours. The accuracy was found to be varied by changing L_s were observed at all three resonant frequencies and the best value chosen is 4.3 mm. The parametric variation of substrate width (W) S_{11} result is revealed in Fig. 11 over the range of frequencies 3 to 6 GHz. The three values are taken for analysing the performance of the S_{11} and those are 26 mm, 27 mm, 28 mm, represented by green, red and blue colours. There is a drastic change in the accuracy, resonant frequencies while changing the width of SIW(W) and also found that increasing the W will increase the accuracy as well as resonant frequency moving toward left that

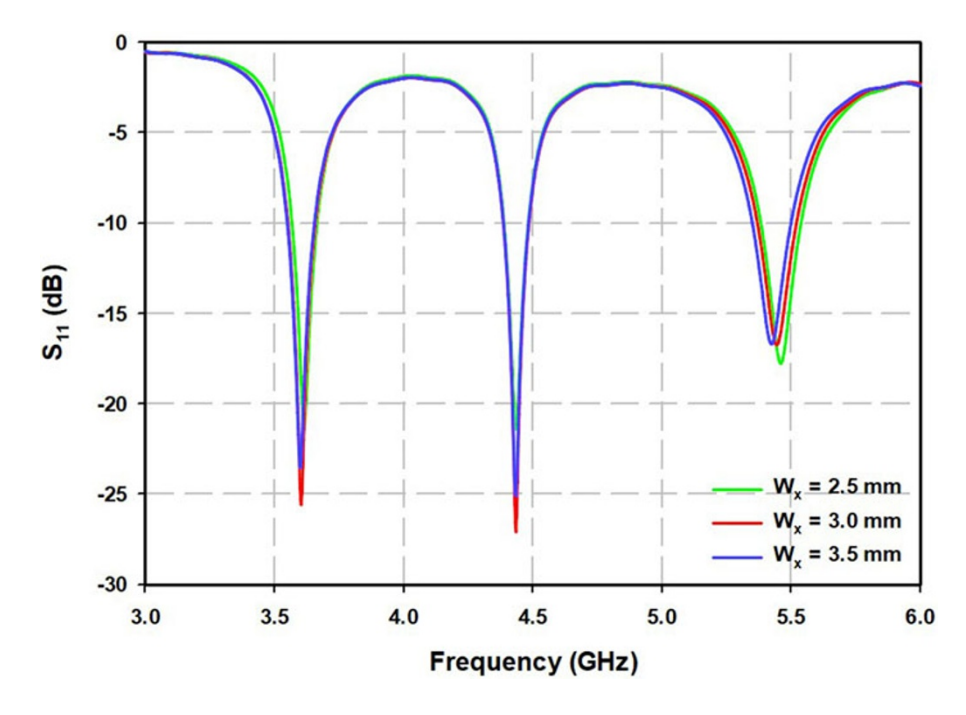


Figure 16. S_{11} for different values of extended substrate width (W_v) .

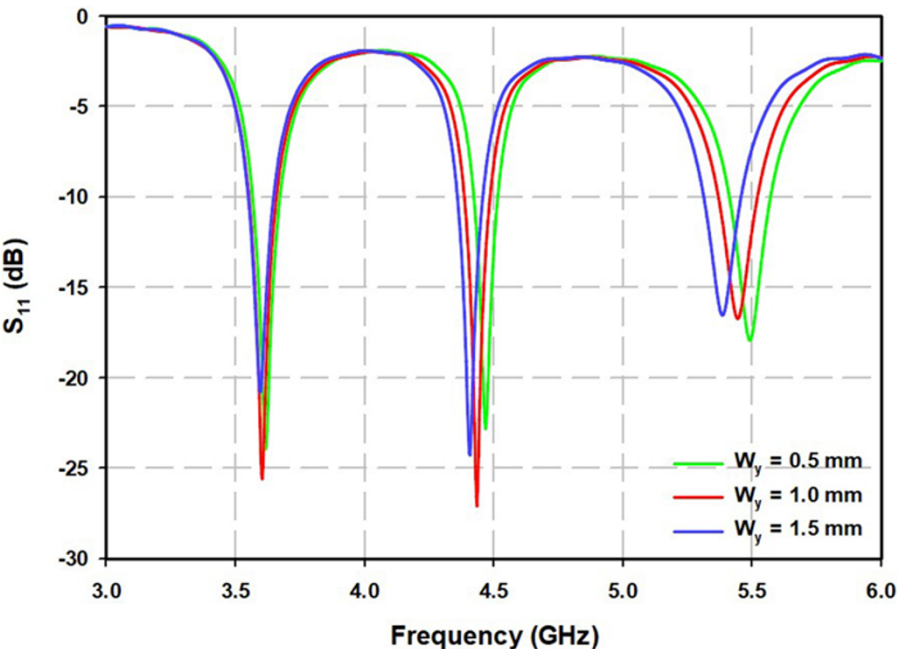


Figure 17. S_{11} for different values of extended substrate length (W_v) .

is decreasing the resonant frequencies and the best value chosen is 27 mm.

The parametric variation of first circle width (W_1) S_{11} result is revealed in Fig. 12 over the range of frequencies 3 to 6 GHz. The three values are taken for analysing the performance of the S_{11} and those are 0.4 mm, 0.5 mm, 0.6 mm, represented by green, red and blue colours. The accuracy was found to be varied by changing W_1 were observed at all three resonant frequencies and also found variations in first resonant frequency. The best value chosen is 0.5 mm.

The parametric variation of octagonal circle width (W_2) S₁₁ result is revealed in Fig. 13 over the range of frequencies 3 to 6 GHz. The three values are taken for analysing the performance of the S₁₁ and those are 0.4 mm, 0.5 mm, 0.6 mm, represented by green, red

and blue colours. The accuracy was found to be varied by changing W_2 were observed at all three resonant frequencies and the best value chosen is 0.5 mm. The parametric variation of second circle slot width S_{11} result is revealed in Fig. 14 over the range of frequencies 3 to 6 GHz. The three values are taken for analysing the performance of the S_{11} and those are 0.4 mm, 0.5 mm, 0.6 mm, represented by green, red and blue colours. The accuracy was found to be varied by changing W_3 were observed at all three resonant frequencies and the best value chosen is 0.5 mm.

The parametric variation of insert feed width S_{11} result is revealed in Fig. 15 over the range of frequencies 3 to 6 GHz. The three values are taken for analysing the performance of the S_{11} and those are 0.7 mm, 0.75 mm, 0.8 mm, represented by green, red and blue colours. The accuracy was found to be varied by changing Ws

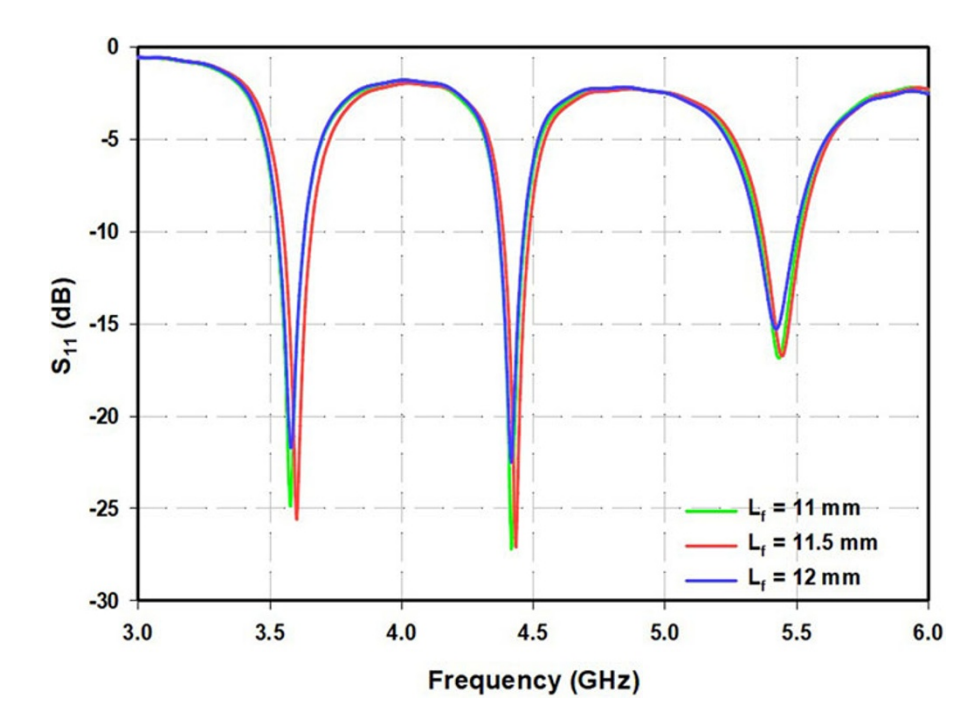


Figure 18. S_{11} for different microstrip feed length (L_f) feed

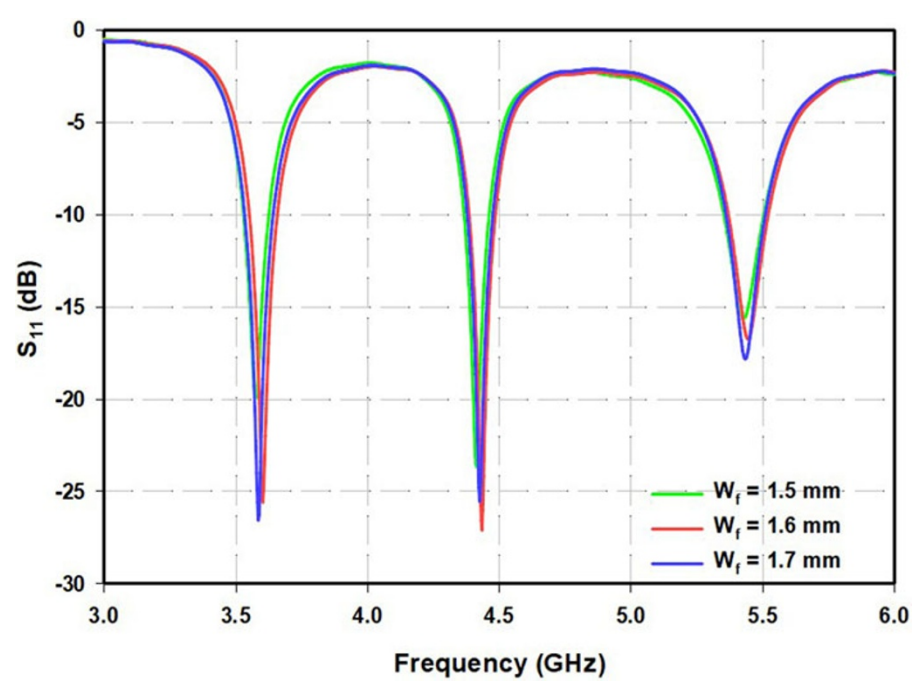


Figure 19. S_{11} for different microstrip feed width $(W_{\rm f})$.

were observed at all three resonant frequencies and the best value chosen is 0.75 mm.

The parametric variation of extended substrate width (W_x) width S_{11} result is revealed in Fig. 16 over the range of frequencies 3 to 6 GHz. The three values are taken for analysing the performance of the S_{11} and those are 2.5 mm, 3.0 mm, 3.5 mm, represented by green, red and blue colours. The accuracy was found to be varied by changing W_x were observed at all three resonant frequencies and also observed variations in third resonant frequency and the best value chosen is 3.0 mm.

The parametric variation of extended substrate width (W_y) width S_{11} result is revealed in Fig. 17 over the range of frequencies 3 to 6 GHz. The three values are taken for analysing the performance

of the S_{11} and those are 0.5 mm, 1.0 mm, 1.5 mm, represented by green, red and blue colours. The accuracy was found to be varied by changing W_y were observed at all three resonant frequencies and also observed variations in second and third resonant frequency and the best value chosen is 1.0 mm.

The parametric variation of microstrip feed length S_{11} result is revealed in Fig. 18 over the range of frequencies 3 to 6 GHz. The three values are taken for analysing the performance of the S_{11} and those are 11 mm,11.5 mm, 12 mm, represented by green, red and blue colours. The accuracy was found to be increased by the feed length with few variations were observed at second and third resonant frequency and the best value chosen is 11.5 mm.

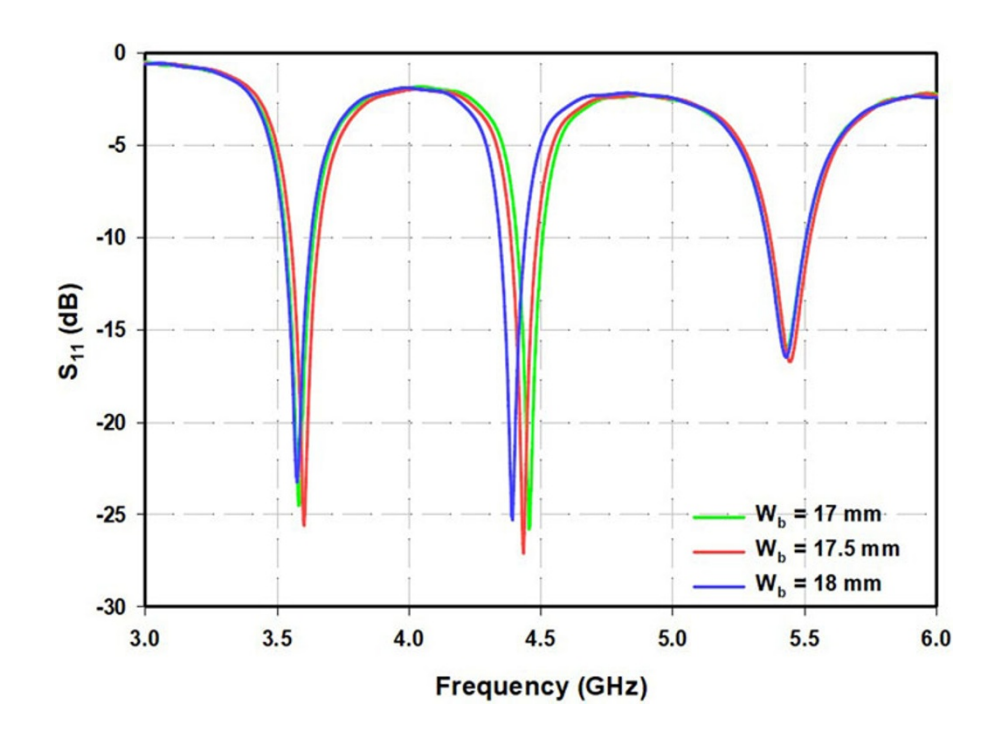


Figure 20. S_{11} for different back slot width (W_b) .

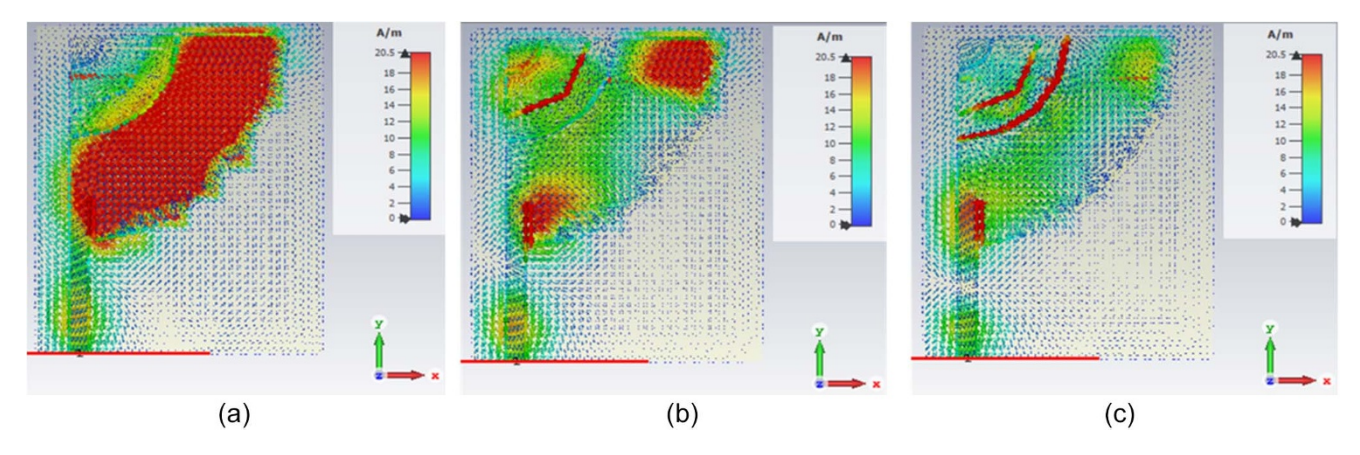


Figure 21. Surface Current. A. 3.57 GHz b. 4.41 GHz. C. 5.43 GHz.

The parametric variation of the microstrip feed width S_{11} result is revealed in Fig. 19 over the range 3 to 6 GHz. The three values are taken for analysing the performance of the S_{11} and those are 1.5 mm,1.6 mm, 1.7 mm, represented using different colours those are green, red and blue colour. The accuracy was found to be increased by the feed width with few variations observed at the first and second resonant frequency and the best value chosen is 1.6 mm.

The reflection coefficient for different values of back side slot width (W_b) is shown in Fig. 20 and three values are chosen to fix the best value of W_b which are 17 mm, 17.5 mm and 18 mm respectively. The change in W_b will affect the antennas second resonant frequency and also accuracy of the first and third resonant frequency. As W_b is increasing second frequency moving to left side and it is improving reflection coefficient. Hence, the optimistic value chosen W_b is 17.5 mm. The surface current of the antenna is shown in Fig. 21 where Fig. 21a, 21b and 21c portray the surface current of the antenna operated at 3.57 GHz, 4.41 GHz and 5.43 GHz respectively. At, 3.57 GHz the current is more on the patch, at 4.41 GHz the current is more at the octagonal slot and

at 5.43 GHz, the surface current is more at the octagonal slot and outer circular slot. In all three frequencies, the current flow is high at the top of the feed point.

The Fig. 22 shows that the comparison of S_{11} in terms of simulated and measured results and as observed compromised results. There is a slight deviation at resonant frequency at 5.6 GHz due to little bit deviations occurred while etching, filling the copper in the holes of the antenna. The measured antenna resonates at 3.57 GHz, 4.41 GHz and 5.6 GHz and their S_{11} values are $-23~{\rm dB}$, $-26~{\rm dB}$ and $-15~{\rm dB}$.

1 X 2 MIMO antenna

A 1×2 MIMO antenna was realized by co-locating a CQMSIW loaded with quarter part octagonal, two-quarter circle on the dielectric substrate. The two radiating elements were arranged in 180 phase differences as shown in Fig. 23 with a gap distance of G_p where the left side structure describes the top view and right-side structure describes bottom view of the structure. The top and bottom views of the fabricated prototype are shown in Fig. 24, and

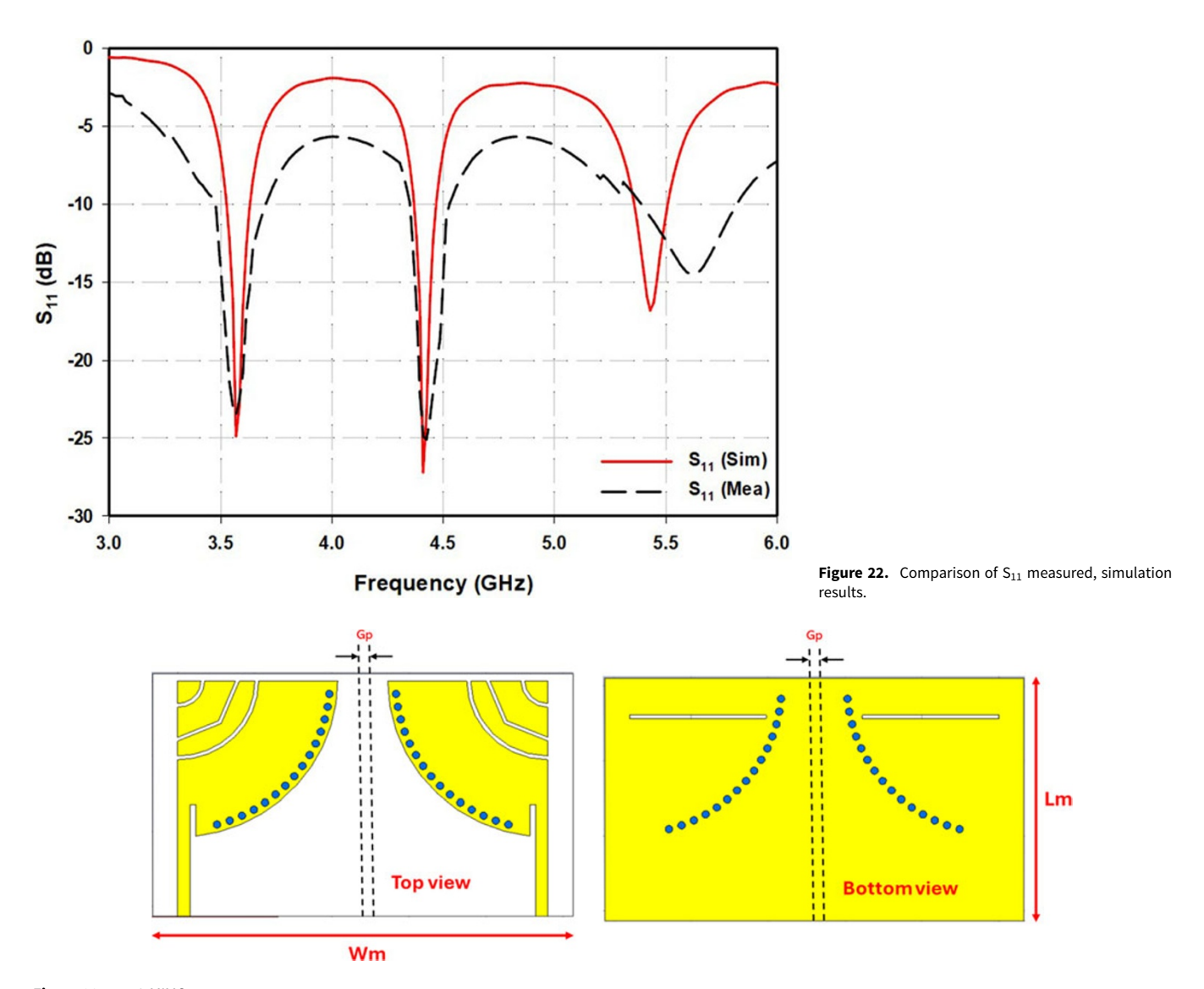


Figure 23. 1×2 MIMO antenna.



Figure 25. Measurement of proposed design using VNA and anechoic chamber.

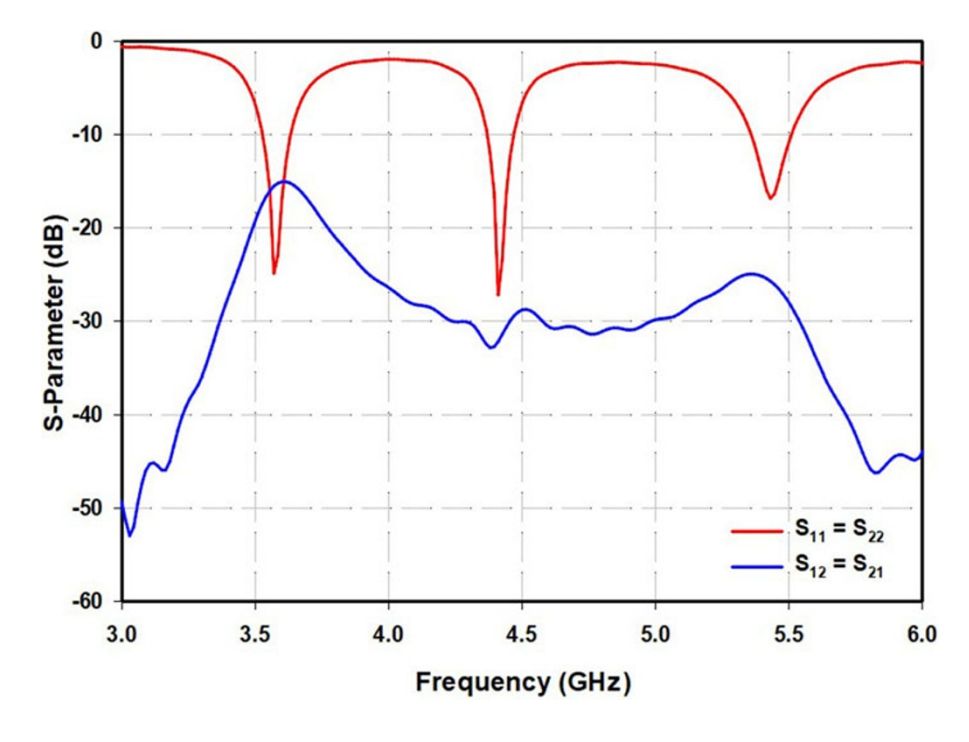


Figure 26. S- Parameters results.

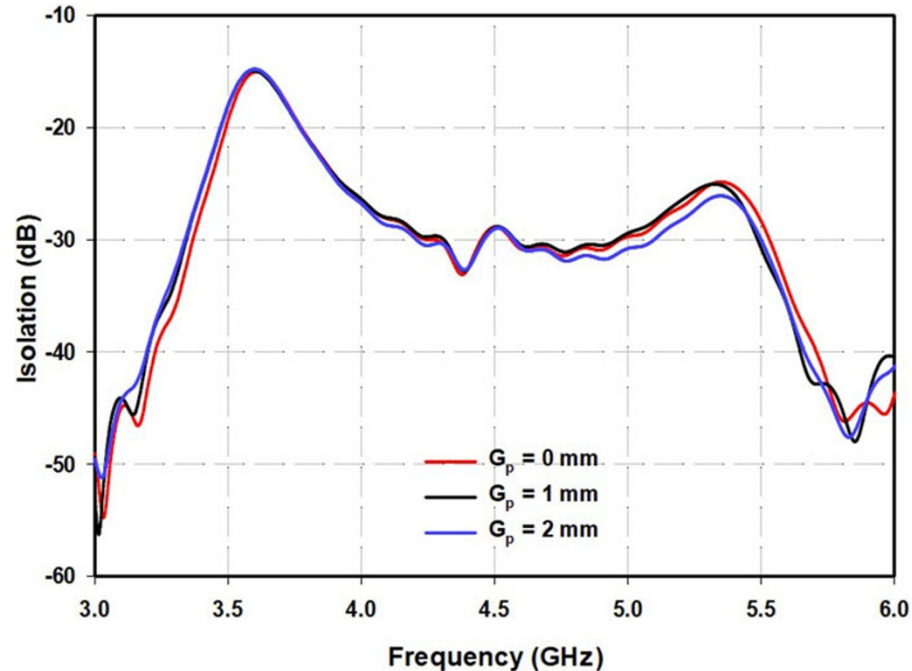


Figure 27. S_{21} values for different values of $G_{p.}$

their dimensions are 54 mm x 33.5 mm x 1.6 mm. The Fig. 25 shows the measured photographs of the antenna where left side indicates VNA setup and right side indicates anechoic chamber.

The S-Parameter of the 1×2 MIMO antenna is shown in Fig. 26 over the frequency range 3 to 6 GHz. The 1×2 is arranged in a symmetric Configuration hence, the S_{11} and S_{22} , S_{12} and S_{21} result are equal. The isolation between the ports is less than (<-15 dB) in simulation results.

The S_{12} result for different values of G_p are reported in Fig. 27. The three different values are chosen to evaluate the best isolation value of the 1 \times 2 array. It is observed that increasing G_P will give better isolation results affecting the accuracy of the

reflection coefficient. From the iteration, the best value chosen is 0 mm.

The comparison of simulation measured S_{11}/S_{12} results are revealed in Fig. 28. The S_{11} results are observed that almost same results in-terms of simulation, measured results except third resonant frequency with respect to -10 dB reference line. The small result fluctuations occurred due to etching the slot. Copper filled in the vias during the fabrication process. There is a compromised results observed in isolation between the ports and the values is less than -15 dB in all the operating frequency band. The Fig. 29 represents the comparison of simulation, measured results in terms of cross and co polarization of the proposed antenna.

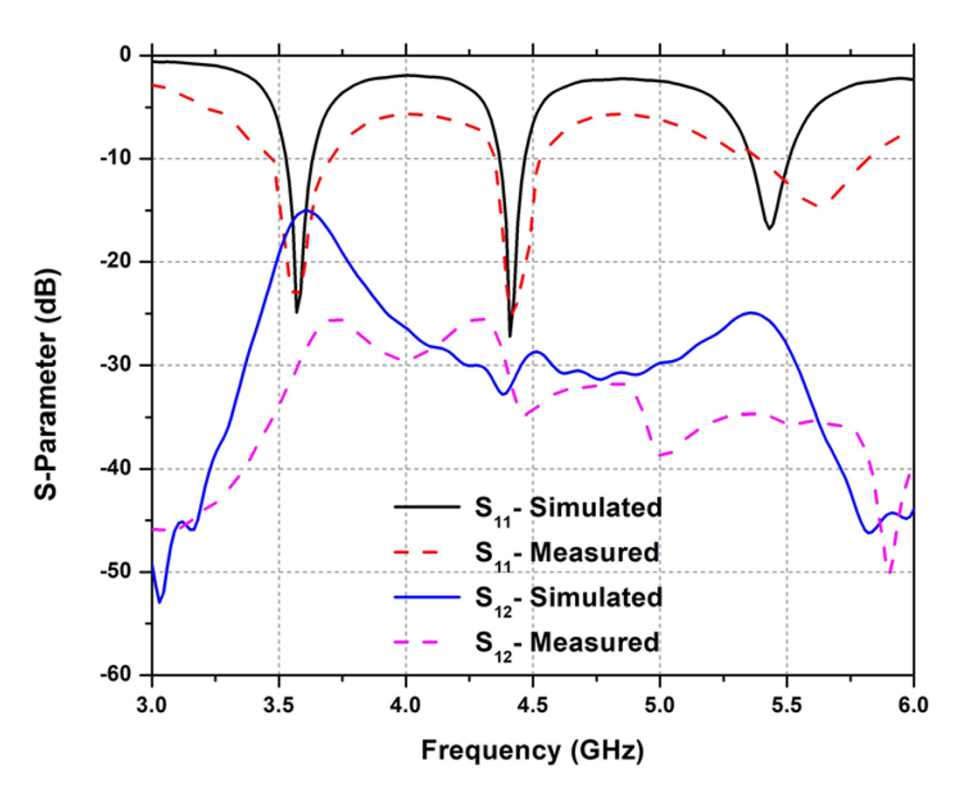


Figure 28. Comparison of S_{11}/S_{21} results.

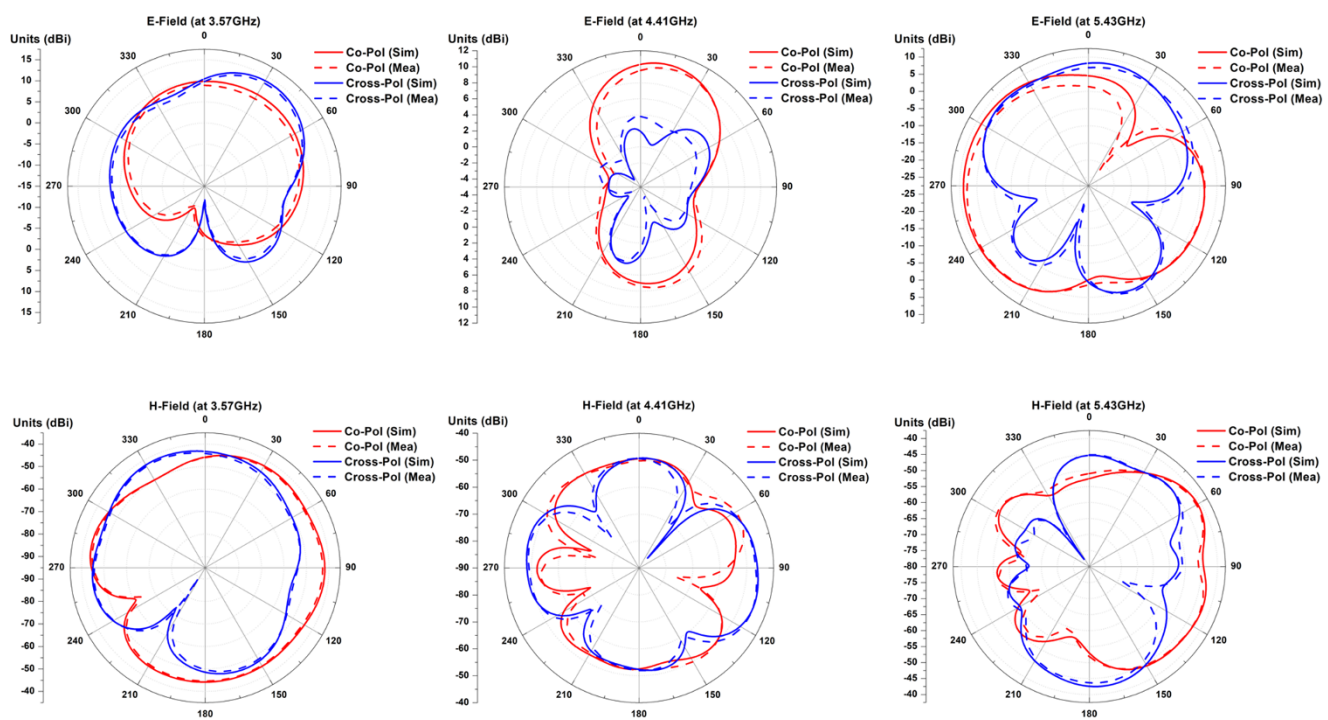


Figure 29. Co and Cross polarization.

The Fig. 29a, Fig. 29b and Fig. 29c shows that E-field and H-field pattern of the proposed antenna at three frequencies those are 3.57 GHz, 4.41 GHz and 5.5 GHz respectively. There is close match between the patterns is observed and radiates bi-directional radiation pattern and well suited the all-commercial wireless applications.

The surface current of the 1×2 MIMO antenna is shown in Fig. 30, which portrays the antenna surface current operated at

3.57 GHz, 4.41 GHz and 5.43 GHz respectively. At 3.57 GHz, the current is more on patch in the port1 and port2; at 4.41 GHz the current is more at the octagonal slot in the port1 and port2 and at 5.43 GHz the surface current is more at the octagonal slot and outer circular slot in the port1 and port2. In all three frequencies, the current flow is high at the top of the feed point. The Fig. 31 shows the comparison of gain results where blue colour indicates simulated results and red colour indicate measured results.

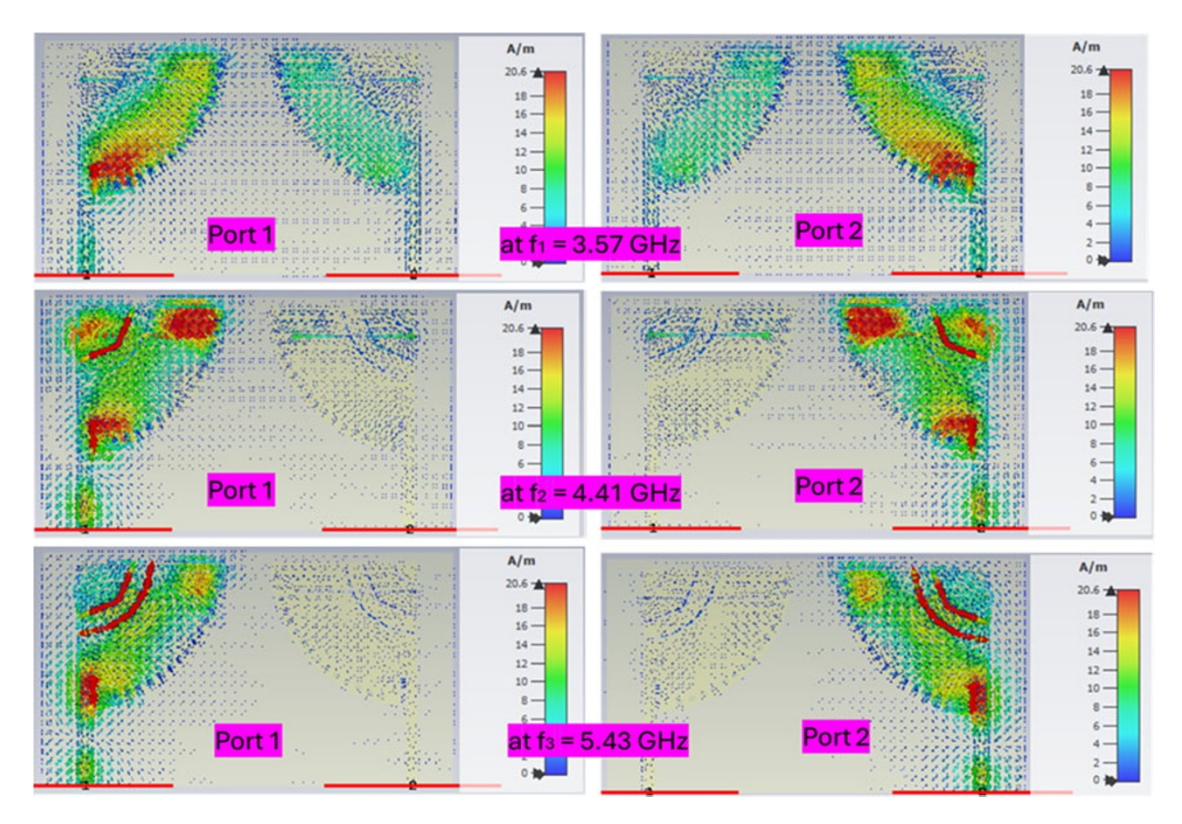
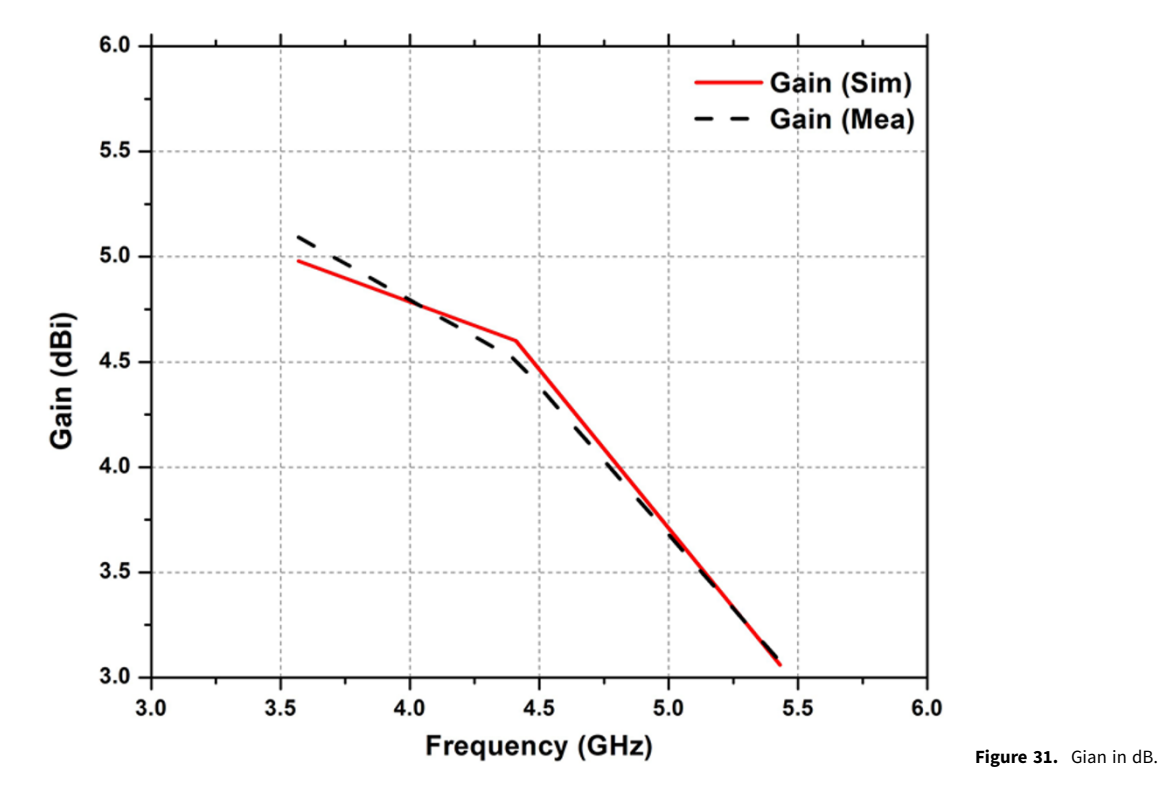


Figure 30. Surface Current of 1×2 MIMO antenna.



The simulated, measured gain values are 4.98dBi, 5.092 dBi, at 3.57 GHz resonant frequency, 4.6dBi, 4.51dBi at 4.41 GHz resonant frequency and 3.06dBi, 3.075dBi at 5.5 GHz resonant frequency. The average gain value is around 4.5dBi in both cases that is sim-

ulation, measured results and well suited operate the applications

like WLAN, WiMAX, Sub 6-GHz, Wi-Fi and fixed wireless access etc.,

The efficiencies of the proposed antenna are represented in Fig. 32 and the blue colour, red colour are indicating radiation and total efficiency. The radiation, total efficiency values are 78%, 76% at

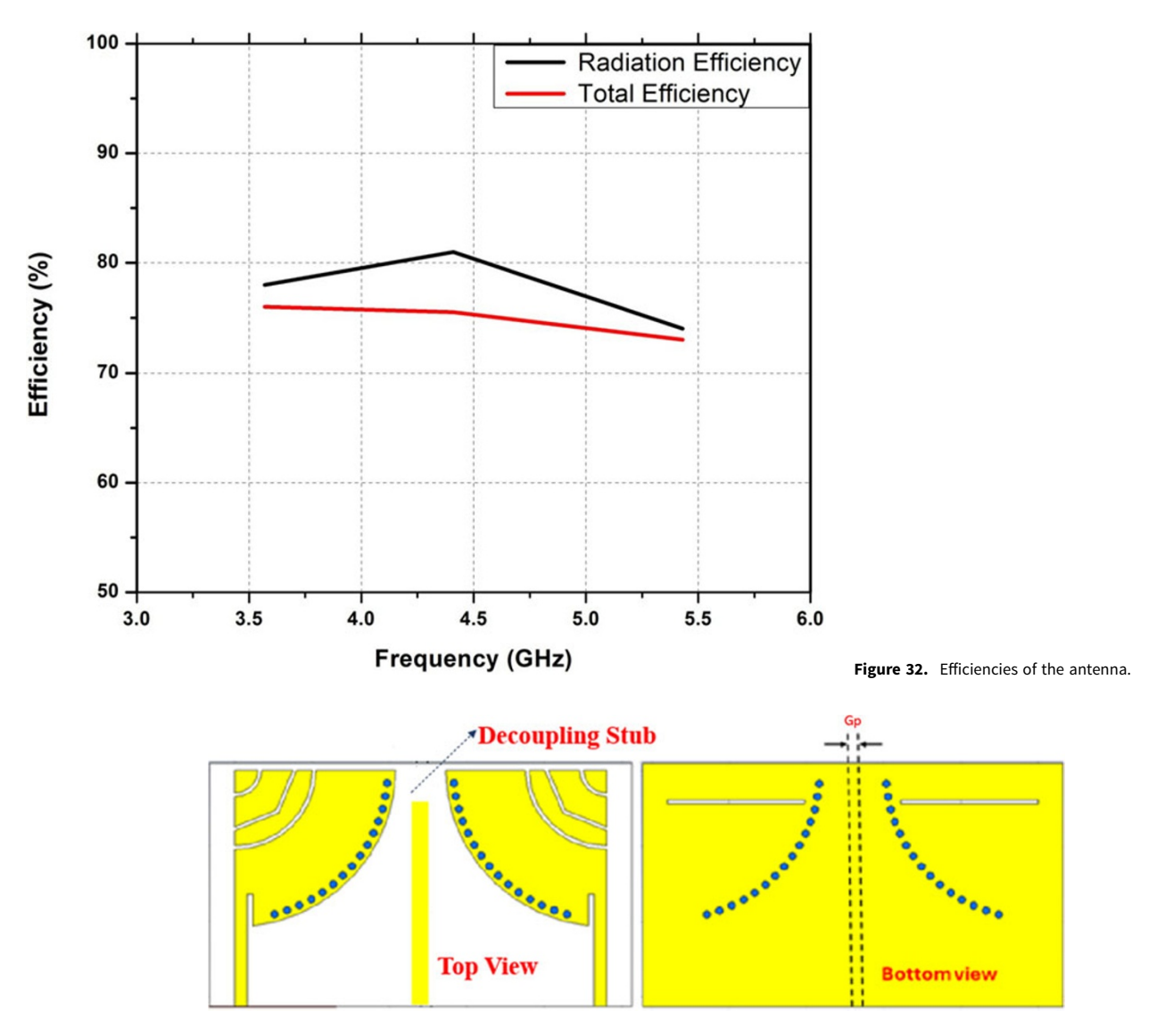


Figure 33. 1×2 MIMO antenna with decoupling stub.

3.57 resonant frequency, 81.02%, 71.5% at 4.41 GHz resonant frequency and 74.1%, 72.89% at 5.43 GHz resonant frequency. This is well suited to operate a wireless application like sub 6 GHz 5 G Applications.

Improvement of isolation at 3.5 ghz

The isolation between the ports is -15 dB at 3.57 GHz resonant frequency and introduces stub between ports to improve the isolation [14] and as represented in Fig. 33. Figure 34 represents the comparison of the S_{12}/S_{21} results with and without stub and as observing there is an improvement in S_{21} results and observed good isolation that is less than -20 dB at first resonant frequency and also observed small variations at other resonant frequencies also.

MIMO Parameters

The ECC, DG and MEG parameters are general parameters to validate the MIMO antenna and their measured result is discussed in preceding sections

Envelope correlation coefficient (Ecc)

The quantity of similarity between the antenna ports with respect to radiated signals is notated as ECC. It computes the similarity or correlation and similarity of the signal envelopes other than the magnitude or phase of signals themselves [14–16].

The ECC value is represented in equation 4 and the ideal value is zero but in practical situations, the tolerable value of ECC is below 0.5. The comparison of simulation measured 1×2 MIMO array ECC is shown in Fig. 35 and observed close match at operating frequency band. From the Fig. 35, observed that ECC value is less than 0.0001 for all the operating frequencies with respect to simulation, measured results.

$$ECC = \frac{\left|S_{11}^{*}S_{12} + S_{22}S_{21}^{*}\right|^{2}}{\left(1 - \left|S_{12}\right|^{2} - \left|S_{22}\right|^{2}\right) \left(1 - \left|S_{12}\right|^{2} - \left|S_{22}\right|^{2}\right)} \tag{4}$$

Diversity gain (Dg)

DG is another essential feature to evaluate the performance of the MIMO antenna and is expressed in terms of ECC as represented in the equation 5 [14–16]. If the DG is 10 dB, the SNR or BER will

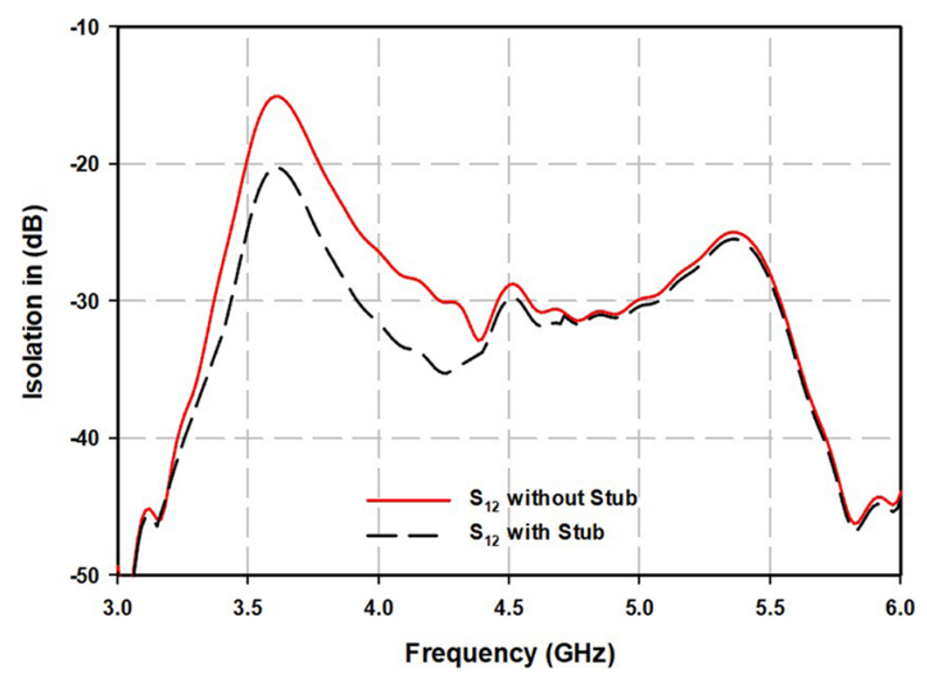


Figure 34. Frequency versus S₁₂/S_{21.}

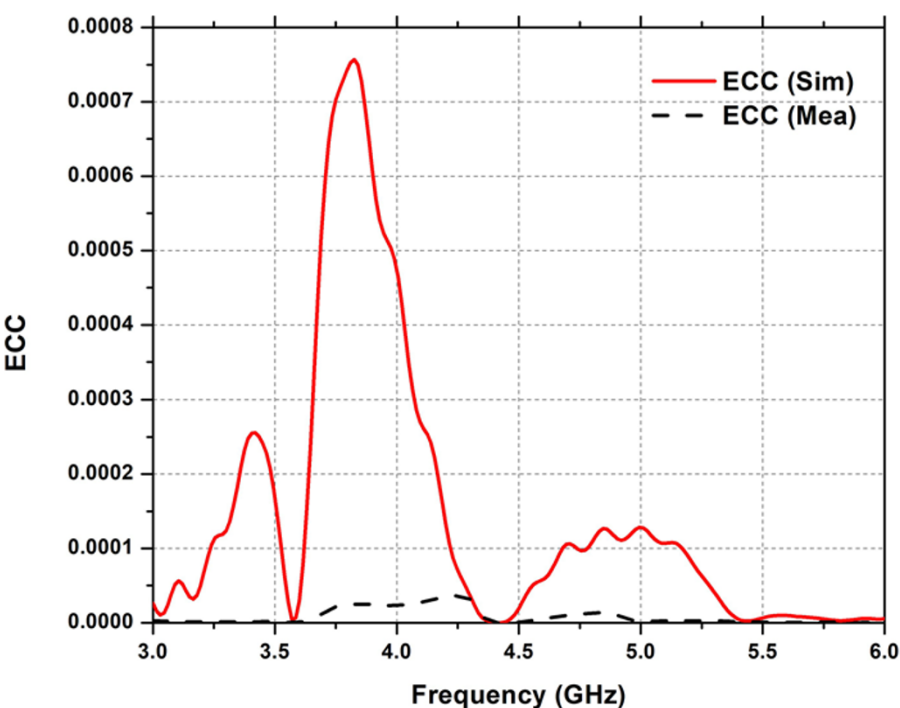


Figure 35. Frequency Vs ECC.

increase by tenfold equated to a single-antenna system. Figure 36 represent the 1×2 HM-SIW based MIMO antenna simulation, measured results and observed close match between simulation, measured results. The DG value is more than 9.995 dB across the operating frequency band.

The proposed antenna has been proven to be effective in combating fading, with less interference and other impairments, reliability, leading to improved signal quality, and overall system performance. The DG and ECC are correlated to each other in an inversely proportional relation, indicating that and that indicates decreasing ECC will increase the value of diversity gain [10, 11].

$$DG = 10\sqrt{1 - ECC} \tag{5}$$

Mean effective gain (meg)

This is used to measure the gain of the antenna in a desired direction ranging from – 3 dB \leq MEG \leq –12 dB [14–16]. The formula is used to find the MEG is in equation 6. Figure 37 represents the MEG between the ports and observed that it lies under the value –3 dB to –4 dB over the operating frequency band and also observed close match between simulation, measured results at every operating frequency. The ratio of MEG1/MEG2 is equal to 1 due to symmetry deign used in the proposed MIMO design (S₁₁ = S₂₂ & S₂₁ = S₁₂).

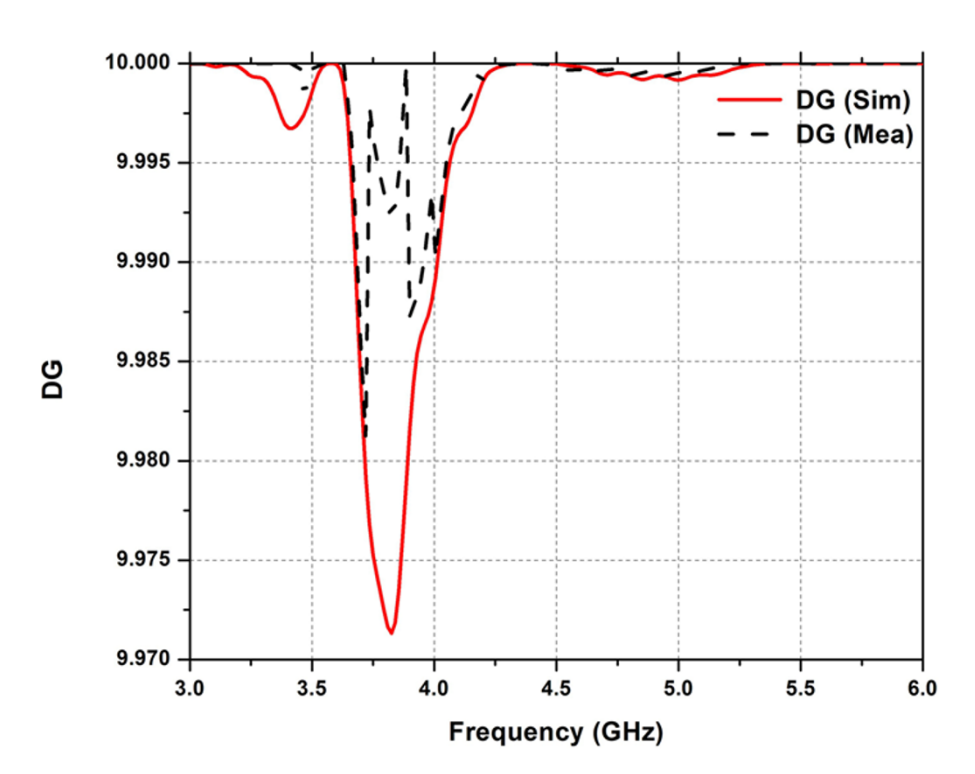


Figure 36. Frequency Vs Diversity Gain (DG).

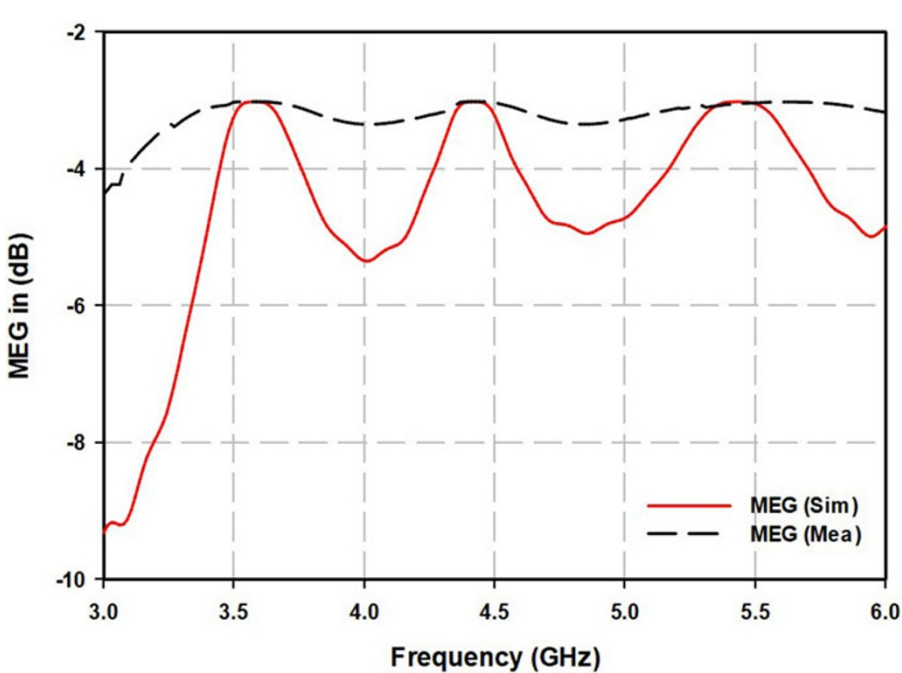


Figure 37. Frequency Vs MEG.

$$MEG_{i} = 0.5 \left(1 - \left|S_{ii}\right|^{2} - \left|S_{ij}\right|^{2}\right)$$
 (6)

Channel capacity loss (Ccl)

Another parameter of to evaluate the performance of MIMO antenna, which tells us the loss occurred during channel. The acceptable value is less than 0.4bits/sec and the equation 7 represents the formulae of CCL

$$CCL = -\log_2 \det \left(\varphi^R \right) \tag{7}$$

$$\varphi^{R} = \begin{pmatrix} \varphi_{ii} & \varphi_{ij} \\ \varphi_{ji} & \varphi_{jj} \end{pmatrix}$$

$$\varphi_{ii} = 1 - \left(\left| S_{ii} \right|^{2} + \left| S_{ij} \right|^{2} \right)$$
(9)

$$\varphi_{jj} = 1 - \left(\left| S_{jj} \right|^2 + \left| S_{ji} \right|^2 \right)$$
(10)

$$\varphi_{ji} = 1 - (S_{jj} * S_{ji} + S_{ij} * S_{jj})$$
(11)

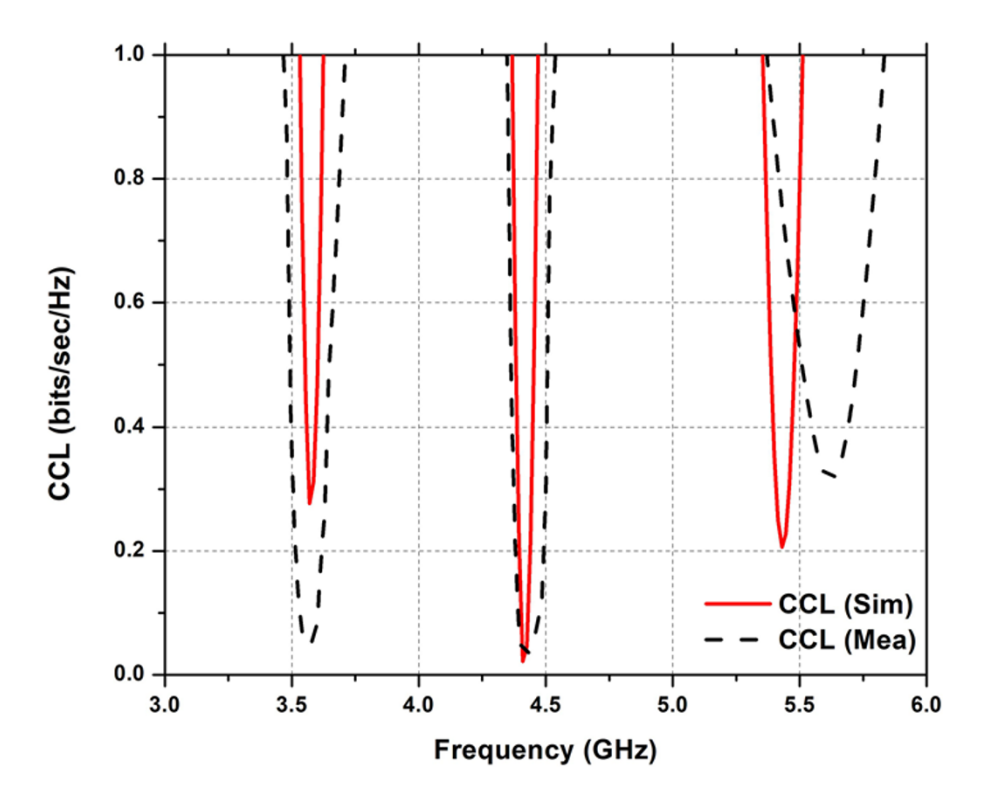


Figure 38. Frequency Vs CCL.

Table 2. Comparison of the proposed work with similar literature

Ref No.	Size (mm³)	No. of Ports	Techniques used	Resonant Frequency (GHz)	Gain in (dBi)	Isolation	ECC	DG
[19]	67.5 x 45x 1.6	2	HMSIW	3.51	5.2	<-15 dB	<0.006	9.95
[20]	21.5 x43x 1.6	2	Elliptical patch	3.5	2.36	<-15 dB	< 0.006	9.998
[21]	31 x 55 x 1.6	2	Frog shaped patch	3.5	-	<-15 dB	<0.006	9.96
[22]	15x15x 6	2	T-shaped monopole and T-shaped slot	3.5/5	3	<-15 dB	<0.01	9.6
[23]	45 x45x 1.59	2	Defected L shaped strip and T shaped stub	3.7/4.8	5.8	<-15 dB	<0.03	9.95
Proposed Work	54 x 33.5 x1.6	2	Circular shaped QMSIW load with slots	3.57/4.4/5.4	4.98/4.6/3.1	< -20 dB	< 0.001	9.995

$$\varphi_{ij} = 1 - \left(S_{ii} * S_{ij} + S_{ji} * S_{ii} \right) \tag{12}$$

The comparison of simulation measured results of CCL as shown in Fig. 38 and observed close match results at every operating frequency. The CCL value is less than 0.3 bits/sec at every operating frequency.

Table 2 represents the comparison of the proposed 1×2 MIMO QMSIW antenna with similar literature in terms of size, technique used in the design, operating bands, number of elements, gain in dBi, efficiency, ECC, DG. The results show that the proposed antenna has achieved moderate gain, size miniaturization, broad bandwidth and good efficiency as compared to existing literature and also observed acceptable MIMO parameters for better isolation.

Conclusion

The quarter mode circle shaped SIW 1×2 MIMO antenna loaded quarter two circular slots, octagonal slot in top view and the rectangular slot in bottom view has been introduced for tri-band sub 6 GHz applications. The microstrip feed with 50 ohms impedance is used; the dimensions are 54 mm x 33.5 mm x 1.6 mm. The simulated using EM tool, FR-4 material is used for printing the design with a height of 1.6 mm, measured and validated by comparing both simulations and measured results. The 1×2 MIMO array has good isolation between the ports that is < -15 dB. The gain of the antenna is 4.98dBi at 3.57 GHz, 4.6dBi at 4.41 GHz, 3.06dBi at 4.9 GHz, stable radiation patterns at all resonant frequency and well suited to operate wireless applications. The ECC value is < 0.0001, MEG value is lies between -3 dB to -4 dB and the DG is around

9.95 dB, which shows that MIMO antenna has maintained good radiation between radiating elements.

Competing interests. The authors report no competing interests.

References

- Deepender M, Shrivastava U and Verma VK, (2021) A study on 5G technology and its applications in telecommunications. International Conference on Computational Performance Evaluation (ComPE), Shillong.
- Niu BJ and Tan JH (2019) Half-mode SIW cavity antenna for Tri-band MIMO applications, *Microwave Optical Technology Letters*, vol. 62, pp. 1697–1701.
- Muhammad RA, Syed MA, Patrizia L and Ernesto L (2023) High performance antenna system in MIMO configuration for 5G wireless communication over sub-6 GHz spectrum. *Radio Science* 58, 1–22.
- Nanda KM and Shanmuganantham T (2019) Broadband I-shaped SIW slot antenna for V-band applications. Applied Computational Electromagnetic Society 34, 1–6.
- Meena RK, Avinash D, Dabhade MK, Srivastava K and Kanaujia BK (2022) Antenna design for fifth generation (5G) applications. URSI Asia-Pacific Radio Science Conference (AP-RASC), India.
- Kumar MK, Yogaprasad K and Anitha VR (2019) A quad-band Sierpenski-based fractal antenna fed by CPW. Microwave and Optical Technology Letters 61, 2342–2347. https://onlinelibrary.wiley.com/doi/10. 1002/mop.32097.
- Muhammad AK, Abdullah GH and Saad HK (2022) mmWave fourelement MIMO antenna for future 5G systems. Applied Sciences 12, 4280–4291. https://doi.org/10.3390/app12094280.
- Kumar MN and Shanmuganantham T (2019) Broadband substrate integrated waveguide Venus-shaped slot antenna for V-band applications. *Microwave and Optical Technology Letters* 61, 2342–2347. https://doi.org/10.1002/mop.31904.
- Soumen B and Susanta KP (2020) Bandwidth improvement of substrate integrated waveguide cavity-backed slot antenna with dielectric resonators. *Microsystem Technologies* 26, 1359–1368. https://doi.org/10.1007/s00542-019.04668-pt/
- Bing JN and Yan JC (2020) Bandwidth-enhanced four-antenna MIMO system based on SIW cavity. *Electronics Letters* 56, 643–645. https://doi. org/10.1049/el.2020.0799.
- Malviya L and Chouhan S (2019) Multi-cut four-port shared radiator with stepped ground and diversity effects for WLAN application. *International Journal of Microwave and Wireless Technologies* 11, 1044–1053. https://doi. org/10.1017/S1759078719000680.
- 12. Nayak VSP and Manjunathachari K (2025) Design and analysis of triband quarter-mode SIW antenna for sub-6GHz, WLAN, and WiFi applications. In Proc. 5th International Conference on Trends in Materials Science and Inventive Materials (ICTMIM), 06–07 February 2025, Kanyakumari, India, pp. 22–25.
- Kamal MM, Yang S, Ren XC, Altaf A, Kiani SH, Anjum MR, Iqbal A, Asif M and Saeed SI (2021) Infinity shell shaped MIMO antenna array for mm-wave 5G applications. *Electronics* 10, 165–166. https://doi.org/10. 3390/electronics10020165.
- Dhananjeyan R, Ramesh S and Kumar DR (2025) Compact octagonal MIMO antenna system for broadband applications with enhanced isolation and wideband performance. *Scientific Reports* 15, 1–13. https://doi. org/10.1038/s41598-025-03494-7.
- Rahman S, Ren XC, Altaf A, Irfan M, Abdullah M, Muhammad F, Anjum MR, Mursal SNF and AlKahtani FS (2020) Nature-inspired

- MIMO antenna system for future mmWave technologies. *Micromachines* 11, 1083. https://doi.org/10.3390/mi11121083.
- Nayak VSP and Manjunathachari K (2025) Compact four-port MIMO high-gain HMSIW slot antenna for sub-6 GHz applications. International Journal of Microwave and Optical Technology 20(3), 281–289
- Murthy N (2020) Improved isolation metamaterial-inspired mm-wave MIMO dielectric resonator antenna for 5G application. *Progress In Electromagnetics Research C* 100, 247–261. https://doi.org/10.2528/ PIERC19112603.
- Sehrai DA, Asif M, Shoaib N, Ibrar M, Jan S, Alibakhshikenari M, Lalbakhsh A and Limiti E (2021) Compact quad-element high-isolation wideband MIMO antenna for mm-wave applications. *Electronics* 10, 1300. https://doi.org/10.3390/electronics10111300.
- Bing JN and Jie HT (2019) Compact two-element MIMO antenna based on half-mode SIW cavity with high isolation. *Progress in Electromagnetics Research Letters* 85, 145–149. https://doi.org/10.2528/PIERL19050103.
- Ramya SG, Suman N and Venkateswara RV (2023) A compact 1
 × 2 MIMO elliptical patch antenna for 5G 3.5 GHz applications. Telecommunications and Radio Engineering 82, 21–30.
- Shanhua Y, Tianchu Y, Xiaorong Q and Xiang L (2025) A frog-shaped UWB MIMO antenna design for 5G. Progress in Electromagnetics Research C 15, 101–112.
- Chang L, Zhang G and Wang H (2021) Dual-band antenna pair with lumped filters for 5G MIMO terminals. *IEEE Transactions on Antennas* and Propagation 69, 5413–5423. https://doi.org/10.1109/TAP.2021. 3060827.
- 23. Jing C, Jianlin H, Bo C, Lingrong S, Tian HL and Gui L (2022) A defected circular ring dual-band MIMO antenna with high isolation for 5G and IEEE 802.11 a/ac/ax. *Progress in Electromagnetics Research M* 113, 237–247. https://doi.org/10.2528/PIERM22080104.



Mr. V. Shiva Prasad Nayak serves as an Assistant Professor in the Department of Electrical, Electronics, and Communication Engineering at GITAM School of Technology, Hyderabad. He is currently pursuing his PhD in Electrical, Electronics, and Communication Engineering at GITAM Deemed to be University, Telangana, India. He holds an M.Tech degree from IIT Kharagpur. With over 14 years of experience

in the teaching profession, Mr. V SHIVA PRASAD NAYAK has contributed significantly to academia through his publications in various journals and conference proceedings. His research interests include antenna, RF, and microwave.



Dr. K. Manjunathachari is a Professor in the Department of Electrical, Electronics, and Communication Engineering at GITAM University, Hyderabad. He earned his Ph.D. from Jawaharlal Nehru Technological University Kakinada (JNTUK) and has over 27 years of academic and research experience. His areas of expertise include Artificial Intelligence (AI) and Signal Processing. Dr. Manjunathachari has published 91 research papers and supervised 18

Ph.D. scholars throughout his career. In addition to his teaching and research activities, Dr. Manjunathachari has authored the book "Signals & Signal Processing Simulation Using MATLAB," published by Canadian Academic Publishing in 2015.